The Plant Cell, Vol. 26: 3709–3727, September 2014, www.plantcell.org

Structural Studies of Cinnamoyl-CoA Reductase and Cinnamyl-Alcohol Dehydrogenase, Key Enzymes of Monolignol Biosynthesis[C][W]

Haiyun Pan,[a,1] Rui Zhou,[a,1,2] Gordon V. Louie,[b,1] Joëlle K. Mühlemann,[c] Erin K. Bomati,[b,d] Marianne E. Bowman,[b] Natalia Dudareva,[c] Richard A. Dixon,[e] Joseph P. Noel,[b,d,3] and Xiaoqiang Wang[a,3,4,5]

[a] Plant Biology Division, Samuel Roberts Noble Foundation, Ardmore, Oklahoma 73401
[b] Howard Hughes Medical Institute, Jack H. Skirball Center for Chemical Biology and Proteomics, The Salk Institute for Biological Studies, La Jolla, California 92037
[c] Department of Biochemistry, Purdue University, West Lafayette, Indiana 47907
[d] Department of Chemistry and Biochemistry, University of California, San Diego, La Jolla, California 92037
[e] Department of Biological Sciences, University of North Texas, Denton, Texas 76203-5017

The enzymes cinnamoyl-CoA reductase (CCR) and cinnamyl alcohol dehydrogenase (CAD) catalyze the two key reduction reactions in the conversion of cinnamic acid derivatives into monolignol building blocks for lignin polymers in plant cell walls. Here, we describe detailed functional and structural analyses of CCRs from *Medicago truncatula* and *Petunia hybrida* and of an atypical CAD (CAD2) from *M. truncatula*. These enzymes are closely related members of the short-chain dehydrogenase/reductase (SDR) superfamily. Our structural studies support a reaction mechanism involving a canonical SDR catalytic triad in both CCR and CAD2 and an important role for an auxiliary cysteine unique to CCR. Site-directed mutants of CAD2 (Phe226Ala and Tyr136Phe) that enlarge the phenolic binding site result in a 4- to 10-fold increase in activity with sinapaldehyde, which in comparison to the smaller coumaraldehyde and coniferaldehyde substrates is disfavored by wild-type CAD2. This finding demonstrates the potential exploitation of rationally engineered forms of CCR and CAD2 for the targeted modification of monolignol composition in transgenic plants. Thermal denaturation measurements and structural comparisons of various liganded and unliganded forms of CCR and CAD2 highlight substantial conformational flexibility of these SDR enzymes, which plays an important role in the establishment of catalytically productive complexes of the enzymes with their NADPH and phenolic substrates.

INTRODUCTION

Lignin is a major structural component of plant cell walls and accounts for ~30% of the organic carbon in the biosphere. It functions to impart both mechanical strength to the cell wall and hydrophobicity to vascular elements and plays an important role in plant development and defense against pathogens (Lewis and Yamamoto, 1990; Whetten and Sederoff, 1995; Boerjan et al., 2003). The polymeric structure of lignin forms from the oxidative coupling of phenylpropenyl alcohols, called monolignols (Boudet et al., 1995). The three prevalent monolignols, *p*-hydroxycinnamyl, coniferyl, and sinapyl alcohol, give rise to hydroxycinnamyl (H), guaiacyl (G), and syringyl (S), respectively, subunits in the lignin polymer. The relative proportion of these three subunits in lignin typically varies according to plant species, tissue type, and developmental stage (Campbell and Sederoff, 1996). In angiosperm lignin, the S- and G-subunits are the most abundant, and these can be joined by at least five different types of linkages (Davin and Lewis, 1992). Lignin content and composition represent key determinants of the physical properties of plant materials, such as the resistance of wood to Kraft delignification (Mellerowicz et al., 2001; Baucher et al., 2003) and the recalcitrance of lignocellulosic biomass to saccharification (Chen and Dixon, 2007).

Monolignol biosynthesis in plants is generally well understood (Anterola and Lewis, 2002; Boerjan et al., 2003), although the potential processing of intermediates along multiple intersecting pathways and the detailed biochemical characterization of the biosynthetic enzymes remain areas of intensive study (Dixon et al., 2001; Donaldson, 2001; Zhou et al., 2010; Lee et al., 2011; Vanholme et al., 2013). The enzymes cinnamoyl-CoA reductase (CCR; EC 1.2.1.44) and cinnamyl alcohol dehydrogenase (CAD; EC 1.1.1.195) catalyze the two key NADPH-dependent reductions in the conversion of cinnamic acid-derived metabolites into monolignols. Typical of most enzymes involved in lignin biosynthesis, both CCR and CAD are found in almost all plant species and are encoded by multiple genes and gene families.

[1] These authors contributed equally to this work.
[2] Current address: Conagen, 15 DeAngelo Dr., Bedford, MA 01730.
[3] These authors contributed equally to this work.
[4] Address correspondence to xiaoqiang.wang@unt.edu.
[5] Current address: Department of Biological Sciences, University of North Texas, Denton, TX 76203-5017.
The authors responsible for distribution of materials integral to the findings presented in this article in accordance with the policy described in the Instructions for Authors (www.plantcell.org) are: Joseph P. Noel (noel@salk.edu) and Xiaoqiang Wang (xiaoqiang.wang@unt.edu).
[C] Some figures in this article are displayed in color online but in black and white in the print edition.
[W] Online version contains Web-only data.
www.plantcell.org/cgi/doi/10.1105/tpc.114.127399

The various isoforms of CCR and CAD may be involved in functionally compensatory or independently regulated pathways for monolignol biosynthesis or, alternatively, in distinct metabolic functions such as defense. Structure-function analyses of these enzymes are essential for delineating their precise biological roles and for understanding evolutionary relationships both within each specific enzyme family and across the broader superfamily of NAD(P)H-dependent reductases.

CCR was identified as the first committed enzyme that directs phenylpropanoid metabolites into the monolignol pathway (Wengenmayer et al., 1976; Lüderitz and Grisebach, 1981). A significant reduction in lignin content resulting from downregulation of CCR expression has been demonstrated in several plant species (Wagner et al., 2013). CCR typically can utilize several distinct hydroxycinnamoyl-CoA thioester substrates, including *p*-coumaroyl-CoA, caffeoyl-CoA, feruloyl-CoA, 5-hydroxyferuloyl-CoA, and sinapoyl-CoA, although most of the characterized CCR isoforms exhibit a kinetic preference for feruloyl-CoA (Li et al., 2005; Zhou et al., 2010). The CCR-catalyzed reduction of a hydroxycinnamoyl-CoA to the corresponding hydroxycinnamaldehyde is distinct from the activity of most reductase/dehydrogenases (which catalyze the interconversion of alcohols and aldehydes or aldehydes and carboxylic acids) and thus represents a mechanistically and technologically important biocatalytic conversion. Primary structure comparisons clearly place CCR within the short-chain dehydrogenase/reductase (SDR) family. However, the three-dimensional structure of a CCR enzyme has not been previously reported.

CAD was identified biochemically initially in soybean (*Glycine max*) (Ebel and Grisebach, 1973; Mansell et al., 1974) and later in many other plant species. With genomic sequences now available for a cadre of plants, a number of CAD-like genes have been identified from *Arabidopsis thaliana* and other plant species (Kim et al., 2004; Barakat et al., 2009). In *Arabidopsis*, 17 genes have been annotated as CAD homologs (Kim et al., 2004), of which only At-CAD5 and At-CAD4 were shown to play major roles in the generation of either coniferyl or sinapyl alcohols for corresponding G- and S-lignin formation, respectively (Sibout et al., 2005). The predominant form of CAD is both NADPH and Zn^{2+} dependent and belongs to the medium-chain dehydrogenase/reductase (MDR) superfamily. The crystal structure of *Arabidopsis* CAD5 has been reported (Youn et al., 2006) and is similar to the structure of an aspen (*Populus tremuloides*) sinapyl alcohol dehydrogenase (Bomati and Noel, 2005) and a putative CAD from yeast (*Saccharomyces cerevisiae*) (Valencia et al., 2004). Both *Arabidopsis* CAD5 and aspen sinapyl alcohol dehydrogenase are homodimeric, with monomeric subunits each carrying a tetrahedrally coordinated catalytic zinc ion in addition to a second structural zinc ion.

Another type of CAD, named abnormal or atypical CAD, has been reported in *Eucalyptus gunnii* and tobacco (*Nicotiana tabacum*; Goffner et al., 1998; Damiani et al., 2005), and a homolog At5g19440 exists in *Arabidopsis*. Because of its low sequence similarity with bona fide CAD, At5g19440 was excluded from the systematic characterization of CADs in *Arabidopsis* (Costa et al., 2003; Kim et al., 2004). However, genetic evidence indicates the involvement of this atypical CAD in lignin biosynthesis in tobacco: RNA interference knockdown of this CAD reduced G-monolignol levels in the noncondensed lignin of transgenic plants (Damiani et al., 2005). In contrast to the classic CAD enzymes described above, these atypical CADs belong to the SDR family (Tanaka et al., 2001). They exhibit enzymatic activities toward the substrates of classic CADs, although their roles in lignin biosynthesis in vivo have yet to be established beyond the one report from tobacco.

Here, we report structural and functional studies/comparisons and evolutionary analysis of CCR and CAD. We first present the three-dimensional structures of both *Petunia hybrida* CCR1 and *Medicago truncatula* CCR2. In addition to elucidating the structural basis for the unusual reduction reaction catalyzed by CCR, these structural models may facilitate rational means to alter the kinetic and selectivity properties of CCR to generate novel monolignols with useful agronomic traits. Second, we identify two CADs from *M. truncatula*, CAD1 and CAD2, which represent a classical and an atypical CAD belonging to the MDR and SDR families, respectively. These enzymes catalyze the reduction of coumaraldehyde, coniferaldehyde, and sinapaldehyde into the corresponding alcohols. Functional characterization and structural analyses together with molecular modeling and docking studies elucidate the specific interactions of Mt-CAD1 and Mt-CAD2 with NADPH and substrates. Structure-based mutagenesis of Mt-CAD2 reveals and confirms the roles of key residues involved in catalysis and substrate binding and affords the engineering of catalytically active variants with increased turnover of sinapaldehyde. Thermal-melting binding assays of CCRs and CADs with substrates extend our understanding of substrate recognition in CCRs and CADs. Finally, structural comparisons of CCRs and CAD2 reveal the conformational dynamics of these enzymes, especially in the cofactor binding region in different catalytic states, and also shed light on how these SDRs evolved to recognize different substrates during the evolution of lignin biosynthesis in the green plant lineage.

RESULTS

Molecular Cloning, Enzyme Activity, and Substrate Preferences of Petunia CCR1 and *M. truncatula* CADs

Petunia CCR1

Petunia genes encoding cinnamoyl-CoA reductase were isolated by BLAST (tBLASTx option) search of a petunia petal-specific EST database (Boatright et al., 2004), the Sol genomics network (http://solgenomics.net), and the Gene Indices at the Dana Farber Cancer Institute (http://compbio.dfci.harvard.edu/tgi/) using two tomato (*Solanum lycopersicum*) CCR homologs, Sl-CCR1 and Sl-CCR2, as query. This search identified three ESTs (two in the petunia EST database, 1.2.G15 and 1.4.A07, and one in the Sol genomics network, SGN-U207925) representing transcripts of a single gene, which based on analyses described here is designated as *CCR1* for cinnamoyl-CoA reductase1.

The coding region of Ph-CCR1 was heterologously expressed in *Escherichia coli* as a hexahistidine-tagged fusion protein. The

recombinant protein was purified by affinity chromatography followed by size exclusion chromatography. The purified Ph-CCR1 protein was assayed with several phenolic-CoA esters (Figure 1, Table 1), including feruloyl-CoA, *p*-coumaroyl-CoA, sinapoyl-CoA, caffeoyl-CoA, and benzoyl-CoA, for catalytic formation of the corresponding phenolic aldehydes. Phenolic aldehyde production was monitored by HPLC. Ph-CCR1 was most active with feruloyl-CoA, followed by sinapoyl-CoA and *p*-coumaroyl-CoA (relative to feruloyl-CoA, 65.4 and 21.6% activity, respectively), and only sparingly active with caffeoyl-CoA and benzoyl-CoA (<1% activity). Detailed kinetic characterization confirmed that Ph-CCR1 exhibits the greatest catalytic efficiency (k_{cat}/K_m) with feruloyl-CoA and sinapoyl-CoA (Table 1). For Ph-CCR1, the observed pH optimum with feruloyl-CoA as substrate was ~6.0, which corresponds closely to optimal pH values previously reported for the CCRs from *E. gunnii* (Goffner et al., 1998), *Populus tremuloides* (Li et al., 2005), *Arabidopsis* (Baltas et al., 2005), and *Leucaena leucocephala* (Sonawane et al., 2013).

The kinetic parameters of Ph-CCR1 were similar to those of *M. truncatula* CCR1, which also exhibits the highest turnover number with feruloyl-CoA and low activity with caffeoyl-CoA (Zhou et al., 2010). A second *M. truncatula* CCR, CCR2, prefers caffeoyl- and *p*-coumaroyl-CoAs. It is likely that Mt-CCR1 is the major CCR involved in lignin biosynthesis, and Mt-CCR2 was proposed to be involved in an alternative route for S lignin biosynthesis in *M. truncatula* (Zhou et al., 2010).

(b) M. truncatula CADs

At least five *CAD* or *CAD*-like genes were identified from the *M. truncatula* gene index (http://compbio.dfci.harvard.edu/tgi/cgi-bin/tgi/gimain.pl?gudb=medicago). Phylogenetic analysis indicated that one tentative contig (TC#118493, referred to hereafter as *CAD1*) is very closely related to the bona fide classic CADs characterized from other plant species (data not shown). Mt-*CAD1* encodes a 358-amino acid protein with 77% identity to *Arabidopsis* CAD5. Another tentative contig (TC#115493, referred to hereafter as Mt-*CAD2*) encodes a 326-amino acid protein that lacks significant sequence similarity to classic CADs (Kim et al., 2004) but is instead more closely related to atypical CADs from *E. gunnii* and tobacco (Goffner et al., 1998; Damiani et al., 2005) and to an uncharacterized *Arabidopsis* gene product (At5g19440).

The aldehyde-reductase activities of heterologously expressed and purified Mt-CAD1 and Mt-CAD2 were measured with three common CAD substrates, coumaraldehyde, coniferaldehyde, and sinapaldehyde (Figure 1). Mt-CAD1 was highly active with all three substrates. By contrast, Mt-CAD2 exhibited relatively modest activity; the turnover rates (k_{cat}) with coumaraldehyde, coniferaldehyde, and sinapaldehyde were only 3, 1, and 0.25%, respectively, of those for Mt-CAD1 (Table 2). The low activity levels of Mt-CAD2 against the common CAD substrates were similar to those of the atypical CAD enzymes from *E. gunnii* (Goffner et al., 1998) and tobacco (Damiani et al., 2005), although Mt-CAD2 was distinct in exhibiting some detectable activity with sinapaldehyde (Table 2). Mt-CAD2 exhibited no activity against feruloyl-CoA and caffeoyl-CoA, two preferred CCR substrates, and taxifolin (dihydroquercetin), a substrate of dihydroflavanol reductase (DFR).

Thermal-Melting Analyses of Ligand Binding Interactions of CCR and CAD

Thermal-melting analyses were used to measure the thermal stabilities of the CCR and CAD proteins and the effects of

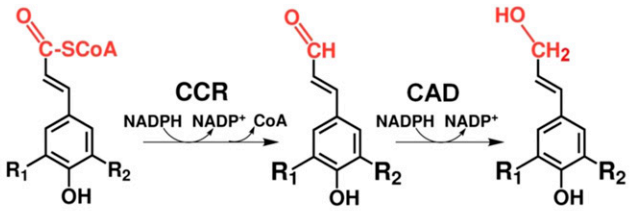

R1=R2=H	p-coumaryl-CoA	p-coumaraldehyde	coumaryl alcohol
R1=OH, R2=H	caffeoyl-CoA	caffeyl aldehyde	caffeyl alcohol
R1=OCH_3, R2=H	feruloyl-CoA	coniferaldehyde	coniferyl alcohol
R1=OCH_3, R2=OH	5-hydroxyferuloyl-CoA	5-hydroxyconiferaldehyde	5-hydroxyconiferyl alcohol
R1=R2=OCH_3	sinapoyl-CoA	sinapaldehyde	sinapyl alcohol

Figure 1. The Monolignol Biosynthesis Reactions Catalyzed by CCR and CAD.

The prevalent conversions occurring in vascular plants (Zhou et al., 2010) are outlined (solid boxes for CCR and dashed boxes for CAD).
[See online article for color version of this figure.]

Table 1. Kinetic Constants of Ph-CCR1 with Various Hydroxycinnamoyl-CoA Esters

Kinetic Parameter	*p*-Coumaroyl-CoA	Feruloyl-CoA	Sinapoyl-CoA
K_m (μM)	208.6 ± 47.4	307.6 ± 9.0	270.3 ± 17.8
V_{max} (nmol mg^{-1} protein s^{-1})	1235.7 ± 168.3	5713.0 ± 66.8	3384.7 ± 111.5
k_{cat} (s^{-1})	1.2 ± 0.3	5.8 ± 0.1	3.4 ± 0.1
k_{cat}/K_m (mM^{-1} s^{-1})	6.0 ± 0.5	18.7 ± 0.3	12.6 ± 0.4

Error values shown are standard errors as derived from nonlinear fit analyses.

various ligands on temperature-dependent unfolding (Table 3). Midpoint protein melting temperatures were measured using a Thermofluor-type assay, which exploits the increased fluorescence of a dye upon interaction with the exposed hydrophobic core residues of an unfolded protein. Although the CCR proteins and Mt-CAD2 share the same tertiary structure, the apo-forms of both Ph-CCR1 and Mt-CCR2 had substantially lower (by ~18°C) midpoint melting temperatures (T_m) than apo-Mt-CAD2.

Effects on T_m of NADP$^+$ and CoA

For both Ph-CCR1 and Mt-CCR2, NADP$^+$ and free CoA individually elicited large positive shifts in T_m (+7 to 10°C and +12°C, respectively), and the two ligands together had an additive stabilizing effect (+17°C). For the two CAD enzymes, Mt-CAD1 and Mt-CAD2, NADP$^+$ induced sizable positive shifts in T_m (+10 to 12°C). Surprisingly, CoA alone also caused (smaller) positive shifts (+4 to 7°C) with both Mt-CAD1 and Mt-CAD2, but in combination, CoA partially negated the stabilizing effect of NADP$^+$. This result can most straightforwardly be interpreted as competitive binding between CoA and the genuine cosubstrate NADP(H), arising from the common molecular features of the two ligands (adenine, ribose with 2/3-phosphorylation, and 5-diphosphorylation).

Effects on T_m of Phenolic-Aldehyde Substrates and Taxifolin

The phenylpropenyl-aldehyde substrates (at 10-fold molar excess and in the presence of NADP$^+$) of Mt-CAD1 and Mt-CAD2 did not significantly affect the thermal stability of either enzyme (in comparison to NADP$^+$ alone). This finding suggests that the binding of these substrates to the CAD enzymes occurs through a relatively small interaction surface and consequently induces little global stabilization of the enzyme. These results for Mt-CAD1 and Mt-CAD2 stand in marked contrast to the substantial stabilization of the CCR proteins by (the substantially larger) free CoA, the carrier of the thioester substrate of CCR. Although not an effective substrate of either Mt-CAD1 or Mt-CAD2, taxifolin (in 20-fold excess and in the presence of NADP$^+$) nevertheless induced a significant positive shift in the T_m of both CAD enzymes.

Structure of Cinnamoyl-CoA Reductase

Overall Structure

The crystal structures of two CCR enzymes were determined: *M. truncatula* CCR2 (Mt-CCR2) in apo form and petunia CCR1 (Ph-CCR1) both in apo form and complexed with NADP$^+$. These two CCRs share 75% amino acid sequence identity and consequently have essentially identical polypeptide chain folds. CCR possesses a bilobal tertiary structure typical of the extended SDR family (Moummou et al., 2012), with distinct NADP (H) binding and substrate binding domains (Figure 2). The NADP (H) binding domain is an alternating α/β structure that forms a seven-stranded, parallel β-sheet (with strand topology 3-2-1-4-5-6-7) sandwiched between two layers of three α-helices. A contiguous region at the N terminus of the polypeptide chain forms the first six β-strands of this β-sheet together with the connecting segments, a structural motif that constitutes a classic Rossmann fold (Rossmann et al., 1975). The seventh β-strand of the NADP(H) binding domain represents a protuberance from the C-terminal substrate binding domain, which folds as a mixed α/β domain with three α-helices, three β-strands, and several extended loop regions. As discussed further below, an extensive active-site cleft resides at the interface between the N- and C-terminal domains.

Binding of NADP(H) to CCR

NADPH, the requisite electron donor (cosubstrate) in the CCR-catalyzed reduction of CoA thioesters (Lüderitz and Grisebach, 1981), interacts with the NADP(H) binding domain of the enzyme through a large number of polar and nonpolar interactions (Figure 3). The following description refers specifically to Ph-CCR1, for which well-ordered binding of the product NADP$^+$

Table 2. Kinetic Constants of Mt-CAD1 and Mt-CAD2 with Various Hydroxycinnamaldehyde Substrates

	Coumaraldehyde		Coniferaldehyde		Sinapaldehyde	
Kinetic Parameter	CAD1	CAD2	CAD1	CAD2	CAD1	CAD2
K_m (μM)	8.0	9.40	8.5	6.60	10.9	730.0000
V_{max} (nmol mg^{-1} protein s^{-1})	402.0	119.00	229.0	27.30	260.0	0.6400
k_{cat} (s^{-1})	15.6	0.46	9.1	0.10	10.2	0.0240
k_{cat}/K_m (mM^{-1}·s^{-1})	1950.0	48.90	1070.0	15.30	926.0	0.0328

Table 3. Effect of Added Ligands on Melting Temperature of Petunia CCR1 and *M. truncatula* CCR1, CAD1, and CAD2 Proteins

	T_m (in °C) in the Presence of Added Ligand				
Protein (10 μM)	None	$NADP^+$ (500 μM)	CoA (1 mM)	$NADP^+$ (500 μM) + CoA (1 mM)	Taxifolin (200 μM) + $NADP^+$ (500 μM)
Ph-CCR1	33	43	45	49	ND
Mt-CCR2	35	42	47	52	ND
Mt-CAD1	52	64	56	62	66
Mt-CAD2	52	62	61	60	64.5

ND, not determined.

was clearly evident (Figure 3A), although the invariance of the amino acid residues involved indicates that the observed NADP(H) binding interactions are conserved in all CCRs (including Mt-CCR2, for which all cocrystallization attempts were unsuccessful). A highly conserved Asp-X-X-Asp motif in all SDRs is known to be important for stabilizing the adenine binding pocket (Filling et al., 2002); in Ph-CCR1, the side-chain carboxylate of Asp-64, the initial Asp of this motif, forms a bridging interaction with the adenine's exocyclic N6-nitrogen and the adjacent Arg-38 guanidinium group (Figure 3A). The adenine ring adopts the anti conformation and is sandwiched between Arg-38 and the side chain of Leu-65. The Gly13-X-X-Gly16-X-X-Ala19 segment, a canonical sequence-motif for NAD(P) binding (Carugo and Argos, 1997), participates in interactions with both the adenine ribose, which is packed against the Cα atoms of both Gly-13 and Gly-16, as well as with the central diphosphate group of $NADP^+$, which forms hydrogen bonds with the backbone amide-nitrogens of residues 17 and 18. The adenine ribose, which adopts the C2′-endo conformation, also interacts through its O4 ring oxygen with the backbone amide-nitrogen of Ser-86. The nicotinamide ribose has the C2′-endo conformation, and its hydroxyl groups are involved in hydrogen bonds with the Thr-84 O, Tyr-157 OH, and Lys-161 NZ atoms of Ph-CCR1. The syn conformation of the nicotinamide ring, which is stabilized by several hydrogen bonds involving the nicotinamide carboxamide group (ON7-187 N, NN7-Ser199 OG, and NN7-NO1 of the $NADP^+$ diphosphate moiety), packs the A-face of the ring against several aliphatic side chains (Ile-18, Pro-184, and Val-187) and directs the B-face toward the binding pocket for the phenolic-CoA ester substrate. In CCR and other closely related NADPH-dependent SDRs, the 2′-phosphate of the adenine ribose is sequestered by a short loop anchored by Arg-38 and Lys-44, which both form salt bridges with the phosphate (Figure 3A). This loop is a key structural feature that distinguishes CCR from the NAD(H)-specific SDRs (Deacon et al., 2000; Filling et al., 2002).

Structural comparisons of the $NADP^+$-complexed form of Ph-CCR1 with the apo forms of both Ph-CCR1 and Mt-CCR2 revealed a number of adjustments that are localized to polypeptide chain segments surrounding the central cleft and are undoubtedly a direct consequence of $NADP^+$ binding (Figure 3B). Consistent with the substantial $NADP^+$-induced stabilization of CCR (Table 3), all of these segments are more ordered structurally in the $NADP^+$-bound form of CCR (as clearly evidenced by lower backbone atomic displacement factors). Most prominently, the connecting loop β4-α4 (Thr84-Pro98) in the $NADP^+$-complexed Ph-CCR1 structure forms interactions with both ribose moieties and represents a central anchoring element for the bound NADP

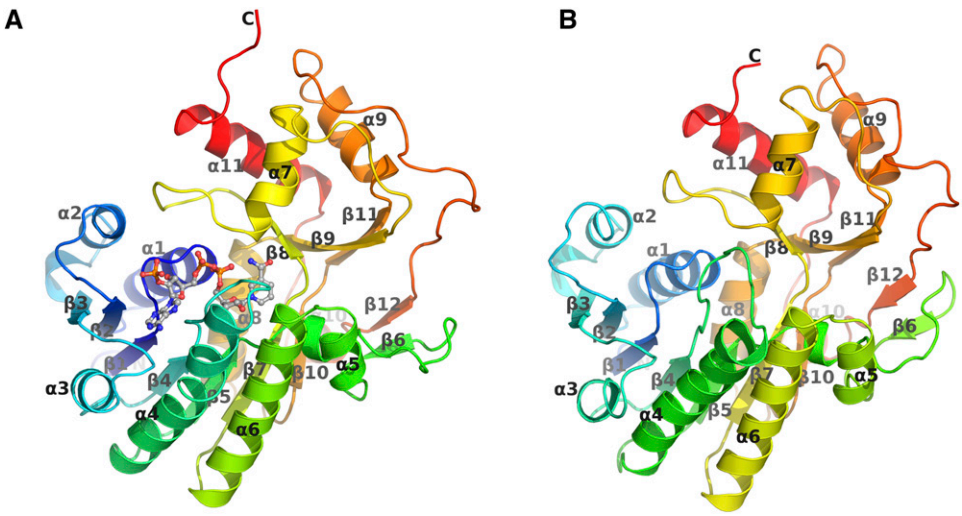

Figure 2. Ribbon Diagrams of the Crystallographically Determined Structures of Ph-CCR1 and Mt-CAD2.

The α-helical, β-strand segments of Ph-CCR1 **(A)** and Mt-CAD2 **(B)** are labeled. $NADP^+$ in Ph-CCR1 is shown in ball-and-stick representation. Figures 2 to 6 were prepared with MOLSCRIPT (Kraulis, 1991) and PyMOL (The PyMOL Molecular Graphics System, version 1.4, Schrödinger).

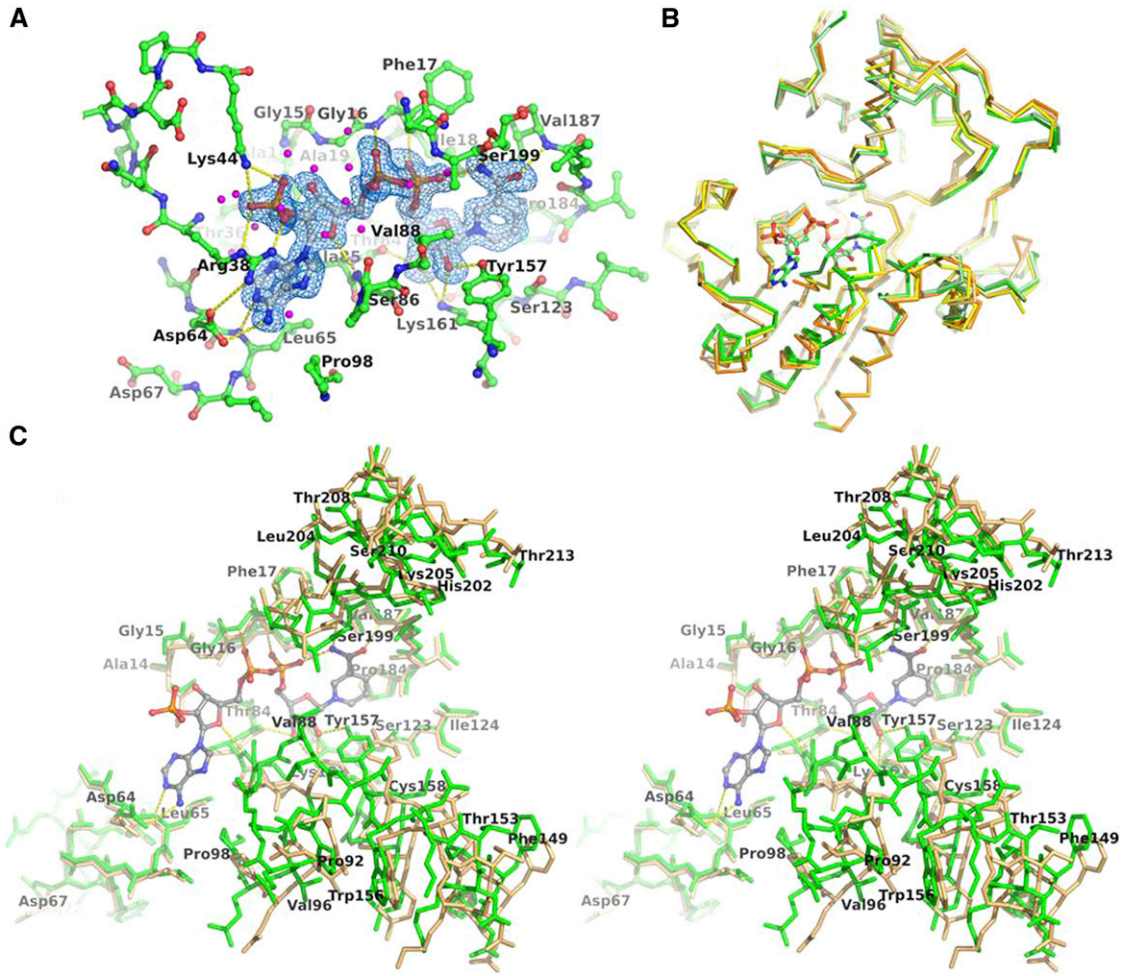

Figure 3. NADP+ Binding by Ph-CCR1.

(A) NADP(H) binding pocket of Ph-CCR1. All protein residues and water molecules contributing an atom within 4 Å of NADP+ are shown. Electron density for NADP+ from an F_o-F_c map (NADP+ omitted from the map calculation) is shown (blue cages, contoured at 3sigma). Water molecules are shown as magenta spheres. All other atoms are shown in ball-and-stick representation and colored according to element (carbon, green for protein atoms, gray for NADP+ atoms; nitrogen, dark blue; oxygen, red; phosphorus, orange). Hydrogen-bond interactions between NADP+ and Ph-CCR1 are shown as yellow dashed-lines.

(B) Structural comparison of polypeptide chain backbone conformations (represented as Cα traces) of the apo and NADP+ bound forms of CCR (green and light green, NADP+-bound Ph-CCR1 molecules A and B; yellow, apo-Ph-CCR1; orange and pale orange, apo-Mt-CCR2 molecules A and B). (The comparisons of the two independent copies in the asymmetric units of apo MtCCR2 and NADP+-bound Ph-CCR1 serve to establish a baseline against which structural differences due to cosubstrate binding can be more reliably discerned.) The two bound NADP+ molecules are shown in ball-and-stick representation (green and light-green carbon atoms).

(C) Detailed view (divergent stereo) of conformational differences in polypeptide chain segments forming NADP(H) binding pocket between the apo- (pale orange) and NADP+-bound (green, molecule A) forms of Ph-CCR1. NADP+ is shown in ball-and-stick representation, with hydrogen-bond interactions between NADP+ and Ph-CCR1 shown as yellow dashed lines.

(H), whereas the corresponding polypeptide chain segment in the two apo-CCR structures is entirely disordered (Figures 3B and 3C). Also apparent are the marked conformational rearrangements and more inward positioning of several regions, in particular residues 63 to 96, 147 to 161, and 197 to 213. These regions contribute key residues that interact with the adenine (Asp-64 and Leu-65), nicotinamide ribose (Tyr-157 and Lys-161), and nicotinamide (Ser-199) moieties of the NADP+ cosubstrate. The combined effect of these structural adjustments is a substantially more closed binding cleft in the NADP+-bound form of CCR.

Inferences on Hydroxycinnamoyl-CoA Binding and Catalytic Mechanism of CCR

Although our crystallographic analyses were successful only in defining the interaction of the NADP(H) cosubstrate with Ph-CCR1, the general features of the further binding of the

hydroxycinnamoyl-CoA substrate to the binary enzyme-$NADP^+$ complex could be largely inferred by docking of hydroxycinnamoyl-CoA into the structure of Ph-CCR1-$NADP^+$ complex. Most restrictively, hydride transfer to the phenylpropenyl-CoA occurs at an internal site within this elongated substrate molecule, and this target site must assume a position adjacent to the nicotinamide ring of the enzyme-bound NADPH. The location of the nicotinamide ring in Ph-CCR1, at the end of a deep cleft, consequently dictates that the hydroxycinnamoyl-CoA substrate is bound with a U-shaped conformation and mostly likely with the phenylpropenyl moiety accommodated within the deepest part of the cleft and the CoA portion folded over and occupying the cleft's outer region (Figure 4). The Ph-CCR1 binding pocket for the phenolic ring is formed by several aliphatic side chains (Ile-124, Gly-125, Val-185, Leu-186, and Ala-220) and is capped by Tyr-284, which is suitably positioned to form a hydrogen bond with the substrate's phenolic (C4) hydroxyl group. The importance for CCR of interactions with the 4-hydroxyl group of the ligand's phenolic ring is demonstrated by the comparatively poorer inhibition by substrate analogs bearing a 4-methoxy modification (Baltas et al., 2005). The putative binding-pocket residues are highly conserved in the CCRs.

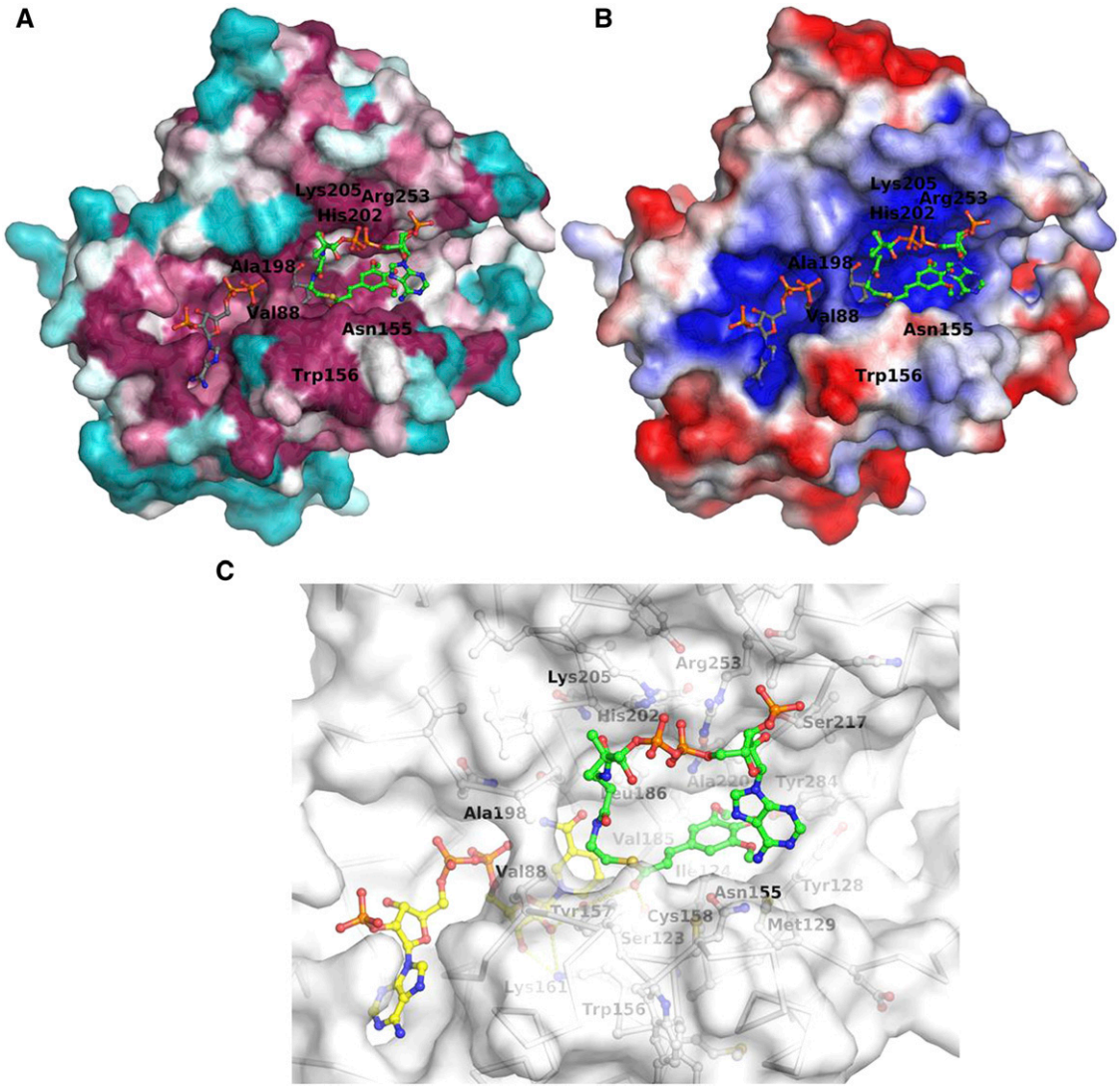

Figure 4. Modeled Binding of Sinapoyl-CoA by Ph-CCR1.

(A) Ph-CCR1 surface colored according to sequence conservation in CCRs (color gradient used is high conservation, purple; average conservation, white; and variable, cyan). Ball-and-stick representations of the $NADP^+$ (yellow carbons) and modeled sinapoyl-CoA (green carbons) are also shown.
(B) Ph-CCR1 surface colored according to electrostatic potential of Ph-CCR1 (color gradient used is +3 kT/e, blue; neutral, white; −3 kT/e, red; as calculated by the Adaptive Poisson-Boltzmann Solver).
(C) Detailed view of sinapoyl-CoA binding pocket in Ph-CCR1. The Ph-CCR1 polypeptide chain is represented by the molecular surface (shown translucent) and by the Cα trace. Protein side chains in the vicinity of the sinapoyl-CoA binding pocket are shown in ball-and-stick representation (light-gray carbon atoms); similarly, $NADP^+$ and sinapoyl-CoA are shown with yellow and green carbon atoms, respectively.

This postulated substrate binding mode is supported by several lines of evidence. In particular, the position in CCR of the phenolic-ring portion of hydroxycinnamoyl-CoA corresponds closely to the binding site of the phenolic B-ring of the dihydroquercetin substrate in dihydroflavonol reductase (Petit et al., 2007). Furthermore, in comparison to the CCR2 homologs of both *Arabidopsis* (Lauvergeat et al., 2001) and *M. truncatula* (Zhou et al., 2010), the CCR1 homologs of these same species are distinguished by a general preference for the more highly substituted phenolic rings of the feruloyl- and sinapoyl-CoA substrates over the smaller caffeoyl- and coumaroyl-CoA substrates. Detailed sequence comparisons identified in both CCR1 homologs a single site at which substitution by a smaller amino acid residue (Ala-225 in At-CCR1 versus Val-219 in At-CCR2, and the equivalent Ala-231 in Mt-CCR1 versus Ser-215 in Mt-CCR2) apparently underlies the differing substrate specificity; notably, this site immediately neighbors the 3 (or 5) substituent (typically a methoxy group, in feruloyl- and sinapoyl-CoA) of the substrate's phenolic ring. Ph-CCR1 likewise bears the smaller Ala-220 residue at this specificity-determining site (Figure 4C), consistent with its preference for the feruloyl- and sinapoyl-CoA substrates (Table 1). Additionally, Mt-CCR2 is distinct from the other CCR homologs in possessing a hydrogen-bonding side chain (Ser-215) at this site and consequently a significant tolerance for caffeoyl-CoA, which bears a hydroxyl group as the 3′ substituent of the phenolic ring. By contrast, At-CCR1, At-CCR2, Mt-CCR1, and Ph-CCR1 carry a residue with an aliphatic side chain (Ala or Val) at the key site and fittingly strongly disfavor caffeoyl-CoA in comparison to feruloyl- and coumaroyl-CoA, which bear more nonpolar substituents (a methoxy group or hydrogen atom, respectively). Indeed, in dihydroflavonol reductase, the corresponding residue, Gln-227, participates in an important hydrogen bond with the 4-hydroxyl group of the dihydroquercetin substrate (Petit et al., 2007).

The CoA portion of the hydroxycinnamoyl-CoA substrate is putatively accommodated within an expansive cleft, which is lined by residues with a markedly high degree of conservation in the CCRs (Figure 4A). A key component of this cleft is the CCR signature sequence motif (KNWYCYGK), which forms a structural scaffold for a segment of polypeptide chain that includes two residues of the catalytic triad and may also participate directly in recognition of the pantetheine moiety of CoA. Additionally, a conserved cluster of basic residues (His-202, Lys-205, and Arg-253 in Ph-CCR1) may have a role in binding the highly electronegative region of the CoA formed by the diphosphate and the 3′-phosphate of the adenine ribose (Figure 4B). Importantly, the CoA portion of the substrate forms interactions that bridge the two domains of the CCR enzyme, a feature that may be responsible for the substantial stabilization of both Mt-CCR2 and Ph-CCR1 induced by free CoA (see below and Table 3). Further crystallographic analyses with stable substrate and transition-state analogs, together with mutagenesis studies, are underway as part of our efforts to fully detail the binding of hydroxycinnamoyl-CoA substrate by CCR.

Typical of enzymes of the SDR superfamily, CCR possesses an active site containing a canonical, Ser-Tyr-Lys catalytic triad (Jörnvall et al., 1995), with the latter two residues residing in the highly conserved Tyr-X-X-X-Lys motif (Jörnvall et al., 1981). Mutagenic analyses of CCR from *L. leucocephala* confirm the absolute requirement of all three residues for enzyme activity (Sonawane et al., 2013). With reference to the modeled ternary complex and modeling study as described above (Figure 4C), the hydroxycinnamoyl-CoA substrate could be seen to be appropriately engaged by both the Ph-CCR1 catalytic triad (Ser123-Tyr157-Lys161) and the NADPH cosubstrate for involvement initially in a classical SDR-mediated hydride transfer. Thus, the side-chain phenolic group of the catalytic Tyr-157 is both the acceptor in a hydrogen bond with the 2′-hydroxyl group of the nicotinamide ribose and the donor in a hydrogen bond with the substrate carbonyl-oxygen adjacent to the site of hydride addition. This carbonyl oxygen also accepts a hydrogen bond from the side-chain hydroxyl group of the active-site Ser-123. The side-chain amino group of the active-site Lys-161 does not interact directly with the substrate, but instead donates hydrogen bonds to both the 2′- and 3′-hydroxyl groups of the nicotinamide ribose. The key hydrogen-bonding network involving Tyr-157, Lys-161, and the bridging 2′-hydroxyl group of the nicotinamide ribose likely functions to modulate the pK_a of the critical Tyr-157 phenolic group. As with typical SDR enzymes, the CCR-catalyzed reduction reaction is initiated with attack on the carbonyl carbon of the thioester substrate by a hydride derived from C4 of NADPH (Filling et al., 2002). The development of a formal negative charge on the carbonyl oxygen is stabilized by a proton donated by Tyr-157 OH (McKinley-McKee et al., 1991) and possibly also by Ser-123 OH (Breton et al., 1996). Subsequent collapse of the tetrahedral (hemithioacetal) intermediate proceeding via cleavage of the carbon-sulfur bond (formerly the thioester linkage) leads ultimately to the release of the products, a phenolic-aldehyde and free-CoA.

The formation of free CoA might be promoted by donation of a proton to the (transiently generated) CoA thiolate, but the identity of the enzyme group (if any) that serves as the proton donor is unclear. The side-chain sulfhydryl group of the absolutely conserved Cys-158 appears to be appropriately positioned to function in this role. However, mutagenic analysis did not unambiguously support the involvement of Cys-158 in catalysis: in comparison to wild-type Ph-CCR1, the relative activity of the Cys158Ser mutant was ~50% lower, but that of the Cys158Ala mutant was ~3-fold higher (Table 4). We are currently investigating further the exact role of this residue, most notably with respect to the participation of Cys-158 in intramolecular disulfide-formation (see also discussion below). Of particular interest is the markedly increased activity resulting from Ala or Ser substitutions of Cys-150 (Table 4). Cys-150 neighbors Cys-158 but is considerably more distant from the catalytic site of the enzyme (Figure 5).

Reversible Disulfide Bond Formation between Cys-150 and Cys-158 in Ph-CCR1

In the crystal structure of the PhCCR1/$NADP^+$ complex, the side chains of two conserved cysteines (Cys-150 and Cys-158) are in close proximity but clearly exist as reduced sulfhydryl groups. By marked contrast, these cysteines form an intramolecular disulfide bond in an alternative crystal form of apo-Ph-CCR1 (in an unliganded state) (Figure 5A). This crystal form serendipitously emerged from crystallization trials of Ph-CCR1 (with CoA), which

Table 4. Activity of Petunia CCR1 Wild-Type and Cys-150/Cys-158 Mutated Forms and the Effect of Mild Oxidation by Sodium Iodide

Ph-CCR1 Enzyme Variant	Specific Activity (pkat/mg Protein)[a]	Effect on Enzyme Activity of Oxidation by Sodium Iodide[b]
Wild type	1122 ± 64	0.570
Cys150Ala	6826 ± 501	0.019
Cys150Ser	5849 ± 133	0.019
Cys158Ala	3759 ± 598	0.750
Cys158Ser	669 ± 30	0.360

[a]Error values shown are SE of the mean.

[b]The values shown represent the activity of the sodium iodide-treated enzyme (0.2 M NaI for 44 h) relative to the activity of the control sample (subjected to the identical treatment except with water in place of the sodium iodide).

identified sodium iodide, a mild oxidizing agent, as a chemical additive that significantly enhanced crystal growth. Measurements of sulfhydryl content subsequently confirmed that the number of equivalents of free thiol per equivalent of Ph-CCR1 was ~5.9 for the native enzyme, but was lowered to ~4.1 after sodium-iodide treatment. (Ph-CCR1 contains nine cysteine residues, but at least three would be considered completely buried in the native apo structure.) Although the intramolecularly disulfide-bonded form of Ph-CCR1 retained the capacity to bind $NADP^+$ (as demonstrated by soaking experiments with apo-Ph-CCR1 crystals and supplemented $NADP^+$), the Cys150-Cys158 disulfide bond perturbs the positioning of two nearby catalytic residues, Tyr-157 and Lys-161 (Figure 5C) and thereby disrupts the hydrogen-bonding interactions of these residues with the nicotinamide ribose of NADP(H). These structural perturbations may underlie the substantively (by ~40%; Table 4) impaired activity of wild-type Ph-CCR1 in the oxidized (disulfide bonded) state. Furthermore, the reversibility of the disulfide-bond formation was evident from the restoration of the reduced states of Cys-150 and Cys-158 in apo-Ph-CCR1 crystals, through incubation with a moderate concentration of dithiothreitol (50 mM, in the absence of sodium iodide) (Figure 5B).

Curiously, the Cys150Ala and Cys150Ser mutants were hypersensitive to inhibition via sodium iodide treatment (Table 4). With these mutant proteins, intramolecular disulfide-bond formation cannot proceed, and reaction with iodide led presumably to the formation a Cys-158 thiol-iodine adduct (Danehy et al., 1971). That such a modification may be responsible for the inhibited activity of the Ph-CCR1-Cys150 mutants is consistent with the known susceptibility of CCR to inhibition by thiol-modifying agents (Goffner et al., 1998; Sonawane et al., 2013).

Structure of Mt-CAD2 and Structural Comparison with CCRs

Overall Structure and Comparisons with CCRs and Other Members of the NADPH-Dependent Short-Chain Dehydrogenase/Reductase Family

The crystal structures of *M. truncatula* CAD2, determined at 2.0-Å resolution (Figure 2B), and Ph-CCR1 (described above) are very similar; superposition gives a root mean square deviation of 1.45 Å with 301 residues aligned and 50% sequence identity (Figure 6A). Sequence comparisons, phylogenetic analyses, and our structure determination nevertheless unambiguously placed Mt-CAD2 within a distinct family (SDR108E/SDR115E; i.e., the SDR108E family together with a SDR115E daughter branch, as proposed by Moummou et al., 2012) of the SDR superfamily. More specifically, Mt-CAD2 resides in the flowering plant phenylacetaldehyde-reductase subgroup, which is notably distinct from the exclusive subgroup formed by the bona fide CCRs. Among SDRs of known structure, Mt-CAD2 also resembles several other enzymes involved in plant flavonoid biosynthesis, namely, DFR (Petit et al., 2007), anthocyanidin reductase (ANR) (Gargouri et al., 2009), and vestitone reductase (VR) (Shao et al., 2007) (41, 33, and 38% sequence identity, respectively) (Supplemental Figure 1). All of these other enzymes also belong to the SDR108E/SDR115E family. In comparison to Mt-CAD2, the root mean square deviation is 2.0 Å for DFR (312 matching residues), 2.3 Å for ANR (277 residues), and 2.5 Å for VR (303 residues) (Figure 6A; Supplemental Figure 1); thus, as expected, the degree of structural similarity between Mt-CAD2 and each of these other SDRs is correlated with the level of sequence identity. Consistent with the disparate substrate specificities of these SDRs, the greatest structural variations are localized to segments of polypeptide chain surrounding the substrate binding pocket of these enzymes (residues 91 to 96, 157 to 163, 136 to 146, 210 to 224, and 278 to 289, Mt-CAD2 numbering) (Figure 6B). Notably, as discussed earlier, the typical substrates of CCR (CoA derivatives) and DFR (taxifolin) apparently can bind to and stabilize Mt-CAD2, although Mt-CAD2 exhibits no activity against these compounds. These results may reflect the acquisition of divergent substrate specificities by the distinct members of these evolutionarily closely related SDRs.

Binding Pockets for NADP(H) Cosubstrate and Phenolic-Aldehyde Substrate in Mt-CAD2

The NADP(H) cosubstrate and phenolic substrate binding sites of an SDR occur within the cleft between the enzyme's two structural domains, as prototypically exemplified in the structure of DFR complexed with NADPH and dihydroquercetin (Petit et al., 2007). Thus, although we obtained a crystallographic characterization only of the apo-enzyme (unliganded) form of Mt-CAD2, useful structural information on NADP(H) and substrate binding by Mt-CAD2 can be readily derived from comparisons with structures of other liganded SDRs (in particular DFR; Figures 6A and 6B), together with molecular docking. The inferred results described below provide a structural basis for a more detailed understanding of the ligand binding and catalytic activities of this less well-characterized class of the CAD enzymes.

NADP(H) Binding and Conformational Dynamics

Structural comparison with $NADP^+$-complexed forms of CCR and DFR demonstrated that Mt-CAD2 adopts a binding mode for this cosubstrate largely identical to that detailed above for CCR (Figure 6C). Interestingly, the connecting loop β4-α4 (Ala87-Tyr91) remains ordered in the Mt-CAD2 apo-enzyme but

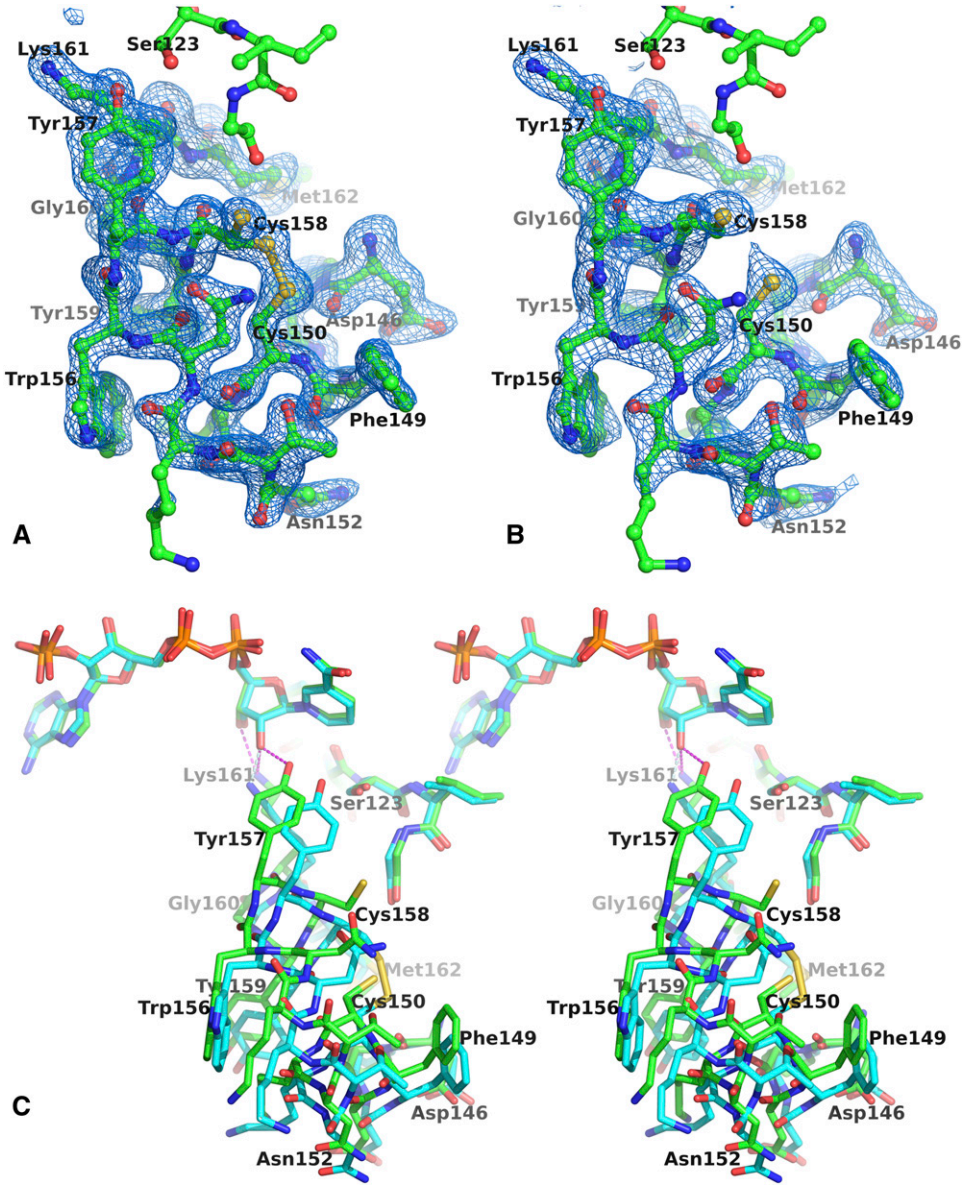

Figure 5. Disulfide Bond Formation between Two Conserved Cysteines, Cys-150 and Cys-158, in Oxidized Ph-CCR1.

(A) Electron density from an F_o-F_c map for a polypeptide-chain segment encompassing the Cys-150/Cys-158 residues is shown (blue cages, contoured at 2sigma; residues 146 to 162 are omitted from the map calculation). Two distinct conformations are observed for the Cys-158 side chain, the first (~35% occupancy) matching that of Cys-158 in native (reduced) Ph-CCR1, and the second (~65% occupancy) with the appropriate positioning of the Cys-158 sulfhydryl-group for disulfide bonding with Cys-150.

(B) The equivalent electron-density map as shown in **(A)** after treatment of the crystals with 50 mM DTT.

(C) Structural comparison (divergent stereo) between the $NADP^+$-bound complexes of the reduced (green carbon atoms) and Cys-150/Cys-158 disulfide-bonded (cyan carbon atoms) forms of Ph-CCR1, highlighting the differences in the polypeptide region spanning residues 150 to 161 and the catalytically important hydrogen-bonding interactions involving Tyr-157, Lys-161, and the $NADP^+$-ribose formed only in the reduced form (shown as magenta dashed lines; except the single interaction involving Lys-161 in the disulfide-bonded form is shown in pale blue).

adopts a conformation that would apparently preclude the typical binding of NADP(H) (in particular, Ser-88 would clash with both the diphosphate and adenosyl-ribose moieties). However, the high temperature factors (~67 $Å^2$, compared with the overall average temperature factor of ~24 $Å^2$) and weak electron density of this segment are indicative of considerable flexibility. As described above, the corresponding region (Pro95-Met103) is likewise disordered in apo-Mt-CCR2 (and also many other SDR enzymes). Additionally, the side chains of Arg-39 and Asn-66 are directed away from the NADP(H) binding cleft in the Mt-CAD2 apoenzyme

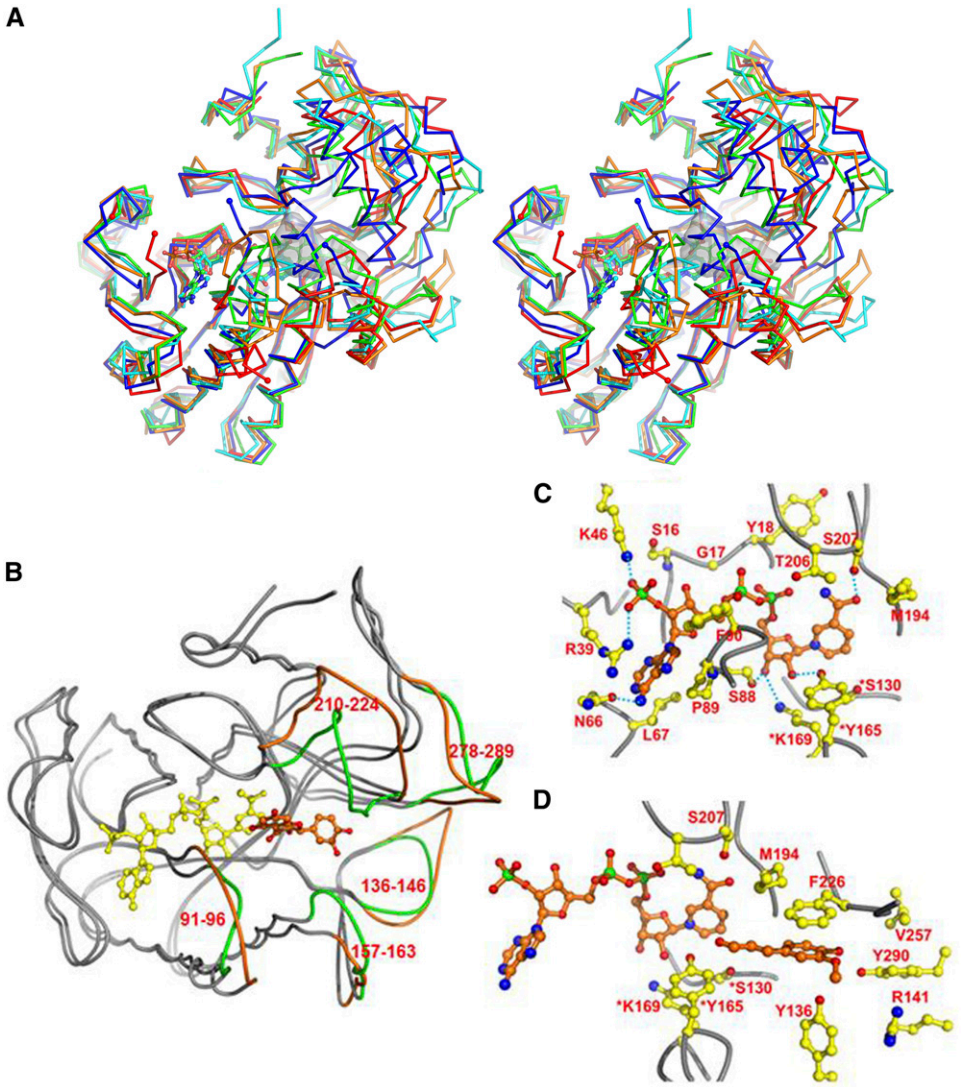

Figure 6. Structural Comparison of the Mt-CAD2 with Other SDR Enzymes.

(A) Structural comparison (divergent stereo) of selected SDRs. Polypeptide-chain backbones are represented as Cα traces: Mt-CAD2 (orange), Ph-CCR1 (cyan), Vv-DFR (green, PDB ID: 2C29), Vv-ANR (blue, PDB ID: 2RH8) and Ms-VR (red, PDB ID: 2P4H). In this view orientation, the NADP(H) binding domains occur at the bottom left and the substrate binding domains occur at the top right (the considerably greater structural variability of the latter domain of the SDRs is evident). The $NADP^+$ occupying the NADPH-cosubstrate binding sites in the Ph-CCR1 (cyan) and Vv-DFR (green) structures is also shown. The binding pocket for the phenolic substrates of these SDRs is highlighted by the gray surface, which is derived from dihydroquercetin bound to the DFR structure. Notable structural variations in the vicinity of the substrate binding pocket of these SDRs include: disordered loops (residues ~91 to 96) in VR and ANR; and the distinct conformation of a lengthy region in ANR (residues 133 to 163, with seven disordered residues). Discontinuities in polypeptide backbones due to internal disordered segments (in the VR and ANR structures) are designated by small spheres marking the bordering ordered residues. **(B)** Superposition of Mt-CAD2 onto DFR containing cofactor and substrate showing the structural variations surrounding the substrate binding pocket. **(C)** and **(D)** Ligand binding pocket in Mt-CAD2 docked with NADPH **(C)** and substrate coniferaldehyde **(D)**. Catalytic triad residues are marked with an asterisk. NADPH, coniferaldehyde, and selected protein residues are shown in ball-and-stick representation.

and must be reoriented to form the expected conserved interactions with NADP(H) (for the Arg-39 guanidinium group, stacking against the adenine purine and a salt bridge to the phosphate group of the adenosyl-ribose 2-hydroxyl; and for Asn-66 OD1, a hydrogen bond to adenine N6). The observed structural differences between the apo and NADP(H)-bound forms of these SDR enzymes directly evidence the important role of localized flexibility in the binding and release of $NADPH/NADP^+$ during the SDR reaction cycle.

Substrate Binding and Specificity of Mt-CAD2

In accordance with the binding by CCR of the phenolic-ester portion of its substrate, the Mt-CAD2 binding site for the

phenylpropene-aldehyde substrate (as identified by docking analyses) occurs at a site adjacent to the *si* face of the NADP(H) nicotinamide, in a pocket formed primarily by hydrophobic side chains (Ile-131, Ala-132, Tyr-136, Ala-193, Met-194, Phe-226, and Tyr-290) (Figure 6D). Positioned at the opposite end of the binding pocket from the NADP(H) nicotinamide, Tyr-290 may provide a hydrogen-bonding partner for the substrate's phenolic (C4) hydroxyl group. Furthermore, the neighboring bulky residues Tyr-136 and Phe-226 apparently dictate sterically the preference of MtCAD2 for phenolic substrates lacking or bearing only a single 3,5-substituent. Thus, the catalytic specificity (k_{cat}/K_m) of Mt-CAD2 was highest for the unsubstituted coumaraldehyde (48.9 $mM^{-1} \cdot s^{-1}$) and the 3-methoxy substituted coniferaldehyde (15.3 $mM^{-1} \cdot s^{-1}$) but markedly lower for the 3,5-dimethoxy substituted sinapaldehyde (0.0328 $mM^{-1} \cdot s^{-1}$) (Table 2). Notably, replacements of Mt-CAD2 Tyr-136 and Phe-226 with smaller residues enhanced activity against sinapaldehyde, with only small changes in catalytic activity against coniferaldehyde. In particular, the catalytic specificity for sinapaldehyde was increased 4-fold in the Mt-CAD2 single-site mutants Tyr136Phe and Phe226Ala and over 10-fold in the combined mutant Tyr136Phe/Phe226Ala (Table 5).

Inferences for the Catalytic Mechanism

Mt-CAD2 contains a canonical SDR catalytic triad, involving Ser-130, Tyr-165, and Lys-169. The absolute requirement for Mt-CAD2 activity of these three residues was confirmed by site-directed mutagenesis: The Mt-CAD2 single-site mutants Ser130Ala, Tyr165Ala, Tyr165Phe, and Lys169Ala all were devoid of activity. In the modeled ternary complex of Mt-CAD2, NADP(H), and coniferaldehyde (Figure 6D), the substrate's C9 aldehyde group is suitably positioned for involvement in the enzyme-catalyzed reduction reaction, for which the proposed roles of each residue of the SDR catalytic triad have been well documented (as detailed further above with the CCR enzyme). In particular, Tyr-165 OH and Ser-130 OG serve as the donors in key hydrogen bonds to the aldehyde oxygen atom. Lys-169, through a hydrogen-bonding network involving also the nicotinamide ribose 2′-hydroxyl group, may participate in a proton shuttle with Tyr-165 OH and act to lower the pK_a of Tyr-165 OH. The reduction reaction proceeds via attack by the nicotinamide-C4 pro-S-hydride (i.e., H_B hydrogen) on the substrate's aldehyde carbon (C9), concomitant with the protonation of the aldehyde oxygen by Tyr-165 OH, thereby generating the phenolic alcohol product.

Structure determination of the apo-form of the Lys169Ala Mt-CAD2 mutant revealed that as a consequence of the loss of the Lys-169 side chain, the side chain of the adjacent catalytic residue Tyr-165 was reoriented, and the extended polypeptide-chain segment (Ser88-Asp93) forming part of the NADPH binding pocket became completely disordered (Supplemental Figure 2). These perturbations localized around the active site may further evidence the structural flexibility that likely plays an important role in ligand binding and enzyme catalysis.

Table 5. Kinetic Constants of Mt-CAD2 Mutants with Sinapaldehyde as Substrate

Mt-CAD2 Protein	K_m (μM)	V_{max} (nmol mg^{-1} Protein s^{-1})	k_{cat} (s^{-1})	k_{cat}/K_m ($\mu M^{-1} \cdot s^{-1}$)
Wild type	730.0	0.64	0.024	32.8
Y136F	279.2	1.02	0.039	139.7
F226A	282.6	1.22	0.044	155.7
Y136F/F226A	234.7	2.18	0.083	353.6
S130A	NDA[a]			
Y165A	NDA			
Y165F	NDA			
K169A	NDA			

[a]NDA, no detectable activity.

Structural Modeling of Mt-CAD1

A homology model of Mt-CAD1 was generated (Supplemental Figure 3A) from the structure of *Arabidopsis* CAD5 (PDB entry 2CF5), which shares 77% sequence identity with Mt-CAD1. These CAD enzymes belong to the MDR family, members of which are characterized structurally by distinct NADP(H) binding (Rossmann-fold) and substrate binding domains as well as a tightly coordinated, catalytic divalent cation (Zn^{2+}). In Mt-CAD1, Zn^{2+} coordination utilizes the side-chain functional groups of four conserved residues, Cys-48, His-70, Glu-71, and Cys-164 (Supplemental Figure 3B). The residues that function in catalysis or in binding of NADP(H) and the phenolic substrate are also nearly invariant between Mt-CAD1 and At-CAD5. One conservative substitution, Ser-50 in Mt-CAD1 for Thr-49 in At-CAD5, occurs at a catalytically important residue that participates in the proton-shuttling network also involving the conserved His-53 and the hydroxyl groups of the nicotinamide ribose of NADP(H).

The substrate binding pocket of Mt-CAD1 is relatively expansive, and consistent with activity measurements (Table 2), all three common phenolic substrates (coumaraldehyde, coniferaldehyde, and sinapaldehyde) can be readily accommodated. By contrast, as discussed above, the binding pocket of Mt-CAD2 appears considerably more restrictive sterically, a feature that may underlie the relatively poor activity of Mt-CAD2 with these phenolic substrates (Table 2).

DISCUSSION

Conserved Catalytic Mechanism of CCR/CAD2 and the Roles of Conserved Cysteine Residues of CCR

Here, we describe functional and structural characterization of two SDR enzymes, CCR and CAD2, which catalyze key reductions in the biosynthesis of monolignols from cinnamic acid-derived building blocks. Our structure determinations and modeling of substrate binding demonstrate that both CCR and CAD2 utilize a reaction mechanism typical of classical SDRs, in which a Ser-Tyr-Lys catalytic triad mediates a hydrogen-bonding network with a crucial role in activating the oxygen of the target carbonyl group and thereby promoting acceptance of a hydride transferred from the nicotinamide of NADPH. CCR is distinguished by an additional activity in promoting the cleavage of a carbon-sulfur bond (formerly the thioester linkage between the hydroxycinnamoyl moiety and CoA) and consequently may require an auxiliary proton donor for the thiolate

leaving group. A prototypical SDR reduction, by contrast, requires a proton donor only for the carbonyl oxygen adjacent to the site of hydride addition, a role fulfilled primarily by the catalytic tyrosine. In CCR, a conserved cysteine adjacent to this tyrosine is a possible candidate for the auxiliary proton donor (these catalytic residues are Tyr-157 and Cys-158 in Ph-CCR1). Sequence comparisons indicate that this cysteine is a hallmark of the CCR enzymes (Escamilla-Treviño et al., 2010). Furthermore, the involvement of a cysteine residue in catalysis may explain the sensitivity of CCR to inhibition by thiol-modifying agents such as mercuric ion and *p*-chloromercuribenzoate (Goffner et al., 1998; Sonawane et al., 2013). Although amino acid substitutions of Cys-158 in Ph-CCR1 are demonstrated here to have a marked effect on enzyme activity, the results (in particular the elevated activity of the Cys158Ala mutant of Ph-CCR1) do not support the absolute requirement of Cys-158 in catalysis. Indeed, that a more active CCR enzyme can arise from amino acid substitutions at Cys-158, and importantly also at the invariant Cys-150 (Table 4), suggests that the absolute conservation of these cysteine residues reflects other underlying factors.

Most notably, Cys-158 together with Cys-150 in Ph-CCR1 can participate reversibly in forming a redox-sensitive, intramolecular disulfide bond. Disulfide-bond formation locks CCR in an inactive state and thereby prevents establishment of a catalytically productive complex with NADPH (Figure 3C). This structural organization may explain the observed requirement of reducing agent for maximal activity of CCR (Li et al., 2005) and further emphasizes the pivotal role of conformational flexibility and redox sensitivity in the activity of the CCRs. Although an artifactual occurrence of the observed disulfide bond in Ph-CCR1 cannot be excluded, the strict conservation and close spatial positioning of the two cysteines suggests that reversible disulfide-bond formation and accompanying enzyme inactivation could underlie an important mechanism for the redox regulation of CCR activity in planta. Considering CCR's role in catalyzing the first committed reaction in monolignol biosynthesis, the oxidative inhibition of CCR activity could result in the diversion of phenylpropanoid precursors toward the production of compounds with antioxidant activity, such as hydroxycinnamic acids and flavonoid compounds like rutin and kaempferol (Tu et al., 2010). Disulfide bond-mediated redox switches have been described recently in a number of other proteins (reviewed in Ryu, 2012). In particular, two enzymes involved in sulfur assimilation by plants, adenosine-5′-phosphosulfate (APS) reductase (APSR) and APS kinase (APSK), have been shown to be regulated through a scheme (Ravilious et al., 2012) paralleling that postulated for CCR. These two enzymes have a common substrate (APS) and are regulated reciprocally by disulfide-bond formation, which enhances APSR activity but inhibits APSK activity. Through this control mechanism, APS can be directed by APSR under conditions of oxidative stress toward cysteine and glutathione biosynthesis or alternatively by APSK under nonstress conditions toward a fate as a sulfate donor for secondary metabolite production.

Conservation and Dynamics of Ligand Binding

Remarkably, despite the much larger overall size of the CCR substrate, the binding sites in Mt-CAD2 of the phenylpropenealdehyde substrate and in Ph-CCR1 of the hydroxycinnamoyl moiety of the CoA-thioester are in close correspondence spatially and share a similar nonpolar makeup and a Tyr cap. Notably, mapping to this pocket in both CCR and CAD are residue determinants that confer a preference for substrates bearing a specific substituent pattern at the 3- and 5-positions of the phenolic ring (typically a hydrogen atom, or a hydroxyl or hydroxymethyl group). The structural conservation of this binding pocket in CCR and CAD2 reflects most obviously the divergence of CCR and CAD2 from a progenitor reductase enzyme that was specific for a phenolic compound. Such an evolutionary ancestry is consistent with the predominance in the SDR108E/SDR115E family of enzymes that participate in phenylpropanoid and flavonoid metabolism (Moummou et al., 2012). Thus, the apparent binding by the CAD enzymes of taxifolin (a substrate of dihydroflavonol reductase, an enzyme belonging to the SDR115E branch) is likely due to recognition of the phenolic ring and propanaldehyde substituent in common with the true phenylpropenyl-aldehyde substrates. Nevertheless, the involvement of alternative, convergent evolutionary pathways cannot be ruled out. In comparison to CCR, Mt-CAD2 lacks both a deep cleft for accommodation of a long CoA moiety and a cluster of conserved basic residues (His-202, Lys-205, and Arg-253 in Ph-CCR1) for interaction with the CoA phosphate groups. These key structural features distinguish the CCRs from the CAD2s and are undoubtedly the primary determinants of the distinct gross substrate specificities of these enzymes.

Thermal denaturation measurements and structural comparisons of unbound and liganded forms of CCR and CAD2 evidence substantial conformational flexibility of these SDR enzymes. The unliganded forms of Ph-CCR1 and Mt-CCR2 in particular have an unusually low melting temperature), reflecting perhaps a general instability associated with the unoccupied, expansive clefts that serve to accommodate two large substrate molecules. Accordingly, both $NADP^+$ and CoA significantly enhance the thermal stability of CCR, indicative of their extensive interaction surfaces with the enzyme. Furthermore, the marked stabilization elicited by CoA possibly correlates with a positioning of bound CoA that bridges the two domains of the enzyme. Comparisons of the structure of $NADP^+$-bound Ph-CCR1 with apo forms of Ph-CCR1, Mt-CCR2, and Mt-CAD2 directly reveal the conformational rearrangement and ordering of several polypeptide chain segments that form the NADP(H) binding cleft (Figures 3C and 6A; Supplemental Figure 4). The affected regions include the connecting loop $\beta4$-$\alpha4$, a central anchoring element for the bound NADP(H), and a segment that includes two residues of the catalytic triad (Tyr-X-X-X-Lys). The $\beta4$-$\alpha4$ loop is commonly observed in SDRs to be conformationally restricted only in the presence of bound NADPH/substrate (Kamitori et al., 2005). Notably, the amino acid residues involved in interactions with the NADPH cosubstrate are generally highly conserved among all SDR enzymes and in particular within the SDR108E/SDR115E family. Therefore, the inherent structural flexibility in the vicinity of the active site is apparently a universal feature of SDR enzymes and is likely important both for facilitating the binding and release of NADP(H) during the enzyme's reaction cycle (Clermont et al., 1993) and for establishing the appropriate spatial arrangement of the enzyme's catalytic groups and substrate molecules.

Functional Evolution of CCRs and CAD

CCRs and CAD2 are in the same highly diverse family of the SDR superfamily (SDR108E/SDR115E) but in clearly divergent subgroups; CCRs form an exclusive subgroup, whereas CAD2 homologs reside in the flowering plant phenylacetaldehyde-reductase subgroup. These two subgroups apparently diverged early in the evolution of land plants because each includes representatives from a broad spectrum of plant species (including *Selaginella moellendorffii* and *Physcomitrella patens*) (Barakat et al., 2011; Moummou et al., 2012). The differing properties of CCR and CAD2 are thus illustrative of an interesting evolutionary diversification that has given rise to distinct enzymes catalyzing a similar chemical conversion and recognizing substrates with common features.

We have shown that two reductases from *M. truncatula*, CAD1 and CAD2, can catalyze the same reduction of coumaraldehyde, coniferaldehyde, or sinapaldehyde to yield the corresponding alcohols. Other instances have been documented of two or more unrelated enzymes independently catalyzing the same single-step biochemical transformation. For example, two types of 3-dehydroquinate dehydratase (DHQase), with dissimilar three-dimensional structures (type-I DHQase has an α/β-barrel topology, whereas type-II DHQase has a flavodoxin-like α/β fold), catalyze via distinct mechanisms the same overall dehydration reaction in the shikimate biosynthetic pathway. Gourley et al. (1999) have suggested that the type-I DHQase is more ancient and may have been lost in some species, whereas the type-II DHQase has been recruited more recently from a catabolic pathway (Gourley et al., 1999).

A broad evolutionary analysis of dehydrogenase/reductase superfamilies indicates that SDR-type enzymes originated early, whereas the more complex MDR-type enzymes, especially the zinc-containing forms, apparently emerged later from spillover at the communal pool stage (Jörnvall et al., 2010). Thus, according to this evolutionary scheme, Mt-CAD1 (an MDR) is likely to be of more recent origin than the ancient atypical Mt-CAD2 (an SDR). Paradoxically, whereas Mt-CAD1 (like At-CAD5) has been demonstrated to be essential for lignin biosynthesis (Zhao et al., 2013) and is highly active against the three CAD substrates coniferaldehyde, sinapaldehyde, and coumaraldehyde, Mt-CAD2 exhibits relatively low activity with these substrates (Table 2) and may therefore have only a secondary role in the production of lignin precursors. Mt-CAD2 may instead compensate functionally upon loss of function of the classic CAD enzyme (Mt-CAD1). This compensatory mechanism suggests that Mt-CAD2 has other biological functions in vivo, such as involvement in lignan biosynthesis or the metabolism of an entirely different substrate or set of substrates.

A detailed understanding of the structural determinants underlying the substrate-preference patterns of CCR can be exploited in planta for engineering the production exclusively of specific monolignol types. Likewise, studies are ongoing to fully define the role of Mt-CAD2 in lignification and then the potential utility of engineered variants of Mt-CAD2 in modifying lignin content and composition in plants. For example, the Phe226Ala/Tyr136Phe variant of Mt-CAD2 exhibits enhanced activity with sinapaldehyde but decreased activity with coumaraldehyde and coniferaldehyde, a property that could potentially be useful for promoting the production of S-lignin over G-lignin. Such mutant Mt-CAD2s could be introduced back into plants, in particular lines harboring knockouts of the classic CAD enzyme.

METHODS

Cloning, Expression, and Purification of Enzymes

Medicago truncatula CAD1 and CAD2 were subcloned into the pET28a(+) vector (EMD Millipore), and *M. truncatula* CCR2 and *Petunia hybrida* CCR1 were subcloned into the pHIS8 expression vector derived from pET28a(+) (Jez et al., 2000) (primer sequences for subcloning are listed in Supplemental Table 1). For protein expression, transformed *Escherichia coli* BL21(DE3) or Rosetta2 cells (Novagen) were incubated with shaking at 37°C in Luria-Bertani medium or Terrific broth containing 50 μg/mL kanamycin (and 34 μg/mL chloramphenicol for Rosetta2 cells) until the OD (at 600 nm) reached 0.5 to 1.0, induced with 0.25 or 0.5 mM isopropyl 1-thio-β-galactopyranoside, grown at 16°C for overnight or at 22°C for 6 h, and finally harvested by centrifugation at 9000*g*. Cell pellets were resuspended in lysis buffer A (TNB, 20 mM imidazole, 10% [v/v] glycerol, 1% [v/v] Tween 20, and 10 mM β-mercaptoethanol [β-ME]; TNB is 50 mM Tris-HCl [pH 8.0] and 500 mM NaCl) supplemented with 4 mM benzamidine, 1 mM PMSF, 2 μg/mL leupeptin, and 0.5 mg/mL lysozyme. Following cell lysis with an EmulsiFlex-C5 homogenizer (Avestin) or by sonication and centrifugation at 100,000*g*, the cleared cell lysate was passed over a Ni^{2+}-NTA column (Qiagen) equilibrated in lysis buffer A, which was then washed with 10 bed volumes of wash buffer (TNB, 20 mM imidazole, and 10 mM β-ME). His-tagged protein was eluted with 10 bed volumes of elution buffer (TNB, 250 mM imidazole, and 10 mM β-ME), and the N-terminal His-tag was cleaved by thrombin digestion during a 24-h dialysis against digestion buffer (TNB and 10 mM β-ME) at 4°C. Cleaved protein was isolated by running the dialyzed sample over another Ni^{2+}-NTA column equilibrated in digestion buffer to remove the His-containing peptide and any uncleaved protein, followed by a benzamidine sepharose column to remove thrombin. A Superdex200 or S75 gel filtration column (Amersham) equilibrated in TNB with 2 mM DTT was used to isolate homogeneous protein, which was finally dialyzed against storage buffer (50 mM NaCl, 12.5 mM Tris-HCl, pH 8.0, and 2 mM DTT), concentrated to 10 to 20 mg/mL, and frozen at −80°C.

Seleno-methionine (SeMet)-labeled Mt-CCR2 protein was prepared as described above for the unlabeled protein, except that during protein expression, *E. coli* BL21(DE3) cells were grown in minimal medium supplemented with an amino acid cocktail containing L-SeMet (Sigma-Aldrich) (Doublié, 1997).

Mutagenesis of Mt-CAD2 and Ph-CCR1

Site-directed mutants of Mt-CAD2 and Ph-CCR1 were constructed using the QuikChange strategy (Stratagene). The mutant proteins were expressed and purified as described for the native protein, except the thrombin cleavage was omitted.

Ph-CCR1 Enzyme Assays

Recombinant Ph-CCR1 activity was determined by measuring product formation using an HPLC-based assay. The standard reaction (40 μL) contained 50 mM Bis-Tris, pH 6.0, 300 μM NADPH, 300 μM CoA ester substrate, and 1.59 μg purified Ph-CCR1 protein. The reaction was initiated by the addition of the CoA ester substrate and incubated for 20 min at 25°C before termination with trichloroacetic acid (5% [w/v] final concentration). Reaction product (10 μL) was analyzed by HPLC-diode array detector spectrophotometry. Chromatographic separation was performed with an Agilent 1200 HPLC system and an Agilent Zorbax SB-C18 (4.6 × 150 mm × 3.5 μm) separation column. The feruloyl-CoA, *p*-coumaroyl-CoA, and sinapoyl-CoA substrates were obtained from TransMIT PlantMetaChem.

Kinetic data were evaluated by hyperbolic regression analysis (HYPER.EXE, version 1.00, 1992). Triplicate assays were performed for all data points for kinetic analysis. Product verification was performed by HPLC analysis of authentic standards and comparison of absorption spectra and retention time. Calibration curves for products were obtained with coniferaldehyde and sinapaldehyde. Since the curves for these two products were very similar, they were used to calculate formation of *p*-coumaraldehyde, the standard of which is not commercially available and similar to that described by Escamilla-Treviño et al. (2010). The pH optimum for Ph-CCR1 was determined as described previously (Klempien et al., 2012).

Ph-CCR1 Disulfide Bond Formation and Reduction

Ph-CCR1 protein samples (at 1 to 10 mg/mL and exchanged into storage buffer free of thiol reductant) were subjected to mild oxidation through addition of 0.2 M sodium iodide. The induced disulfide-bond formation was monitored through the quantitation of free sulfhydryl groups (on cysteine side chains) by reaction with 5,5′-dithio-bis-(2-nitrobenzoic acid) (Ellmann's reagent; Sigma-Aldrich), with assumed molar extinction coefficients of 14,150 $M^{-1} \cdot cm^{-1}$ at 412 nm for 2-nitro-5-thiobenzoic acid and 41,370 $M^{-1} \cdot cm^{-1}$ at 280 nm for Ph-CCR1. Sodium iodide treatment was found to result in the loss maximally of two equivalents of free thiol per equivalent of Ph-CCR1 (this level of modification was attained after 44 h but was incomplete after 1 h). For enzyme activity assays of Ph-CCR1 samples that were subjected to oxidation, sodium iodide was removed by ultrafiltration. With crystals of Ph-CCR1 (see below) containing an intramolecular Cys150-Cys158 disulfide bond, reductive cleavage of the disulfide bond was effected by incubation of crystals for at least 8 h each first in mother liquor without sodium iodide and subsequently in mother liquor supplemented with 50 mM DTT.

Mt-CAD Enzyme Assay and Kinetics

Purified enzyme (0.1 μg for Mt-CAD1; 1.0 μg for Mt-CAD2) was incubated in a final volume of 100 μL with assay buffer (100 mM phosphate, pH 6.25, 10 mM β-ME, and 0.2 mM NADPH) and cinnamyl aldehyde substrates at various concentrations. The reaction was performed at 30°C for 30 min and then terminated with the addition of 100 μL methanol. After centrifugation at 16,000*g* for 10 min, the supernatant (25 μL) was subjected to HPLC analysis with a Waters Spherisorb ODS-2 5-μm reverse-phase column (5-μm particle, 250 × 4.6 mm) on a Beckman System Gold HPLC system consisting of a programmable solvent module 126, a System Gold 508 autosampler, and a System Gold 168 diode array detector. Eluted compounds were identified by comparison of UV spectra and chromatographic retention times with those of authentic standards of hydroxycinnamyl alcohols and quantified by means of standard curves with correction for recovery of internal standards. For kinetic analysis at various substrate concentrations, enzyme velocity curves were analyzed using Sigmaplot 10 software (Systat Software).

Thermal-Shift Binding Assay

The shift in melting temperature for CCR and CAD proteins observed under increasing concentrations of ligands was measured using a Thermofluor-type assay similar to one previously published (Niesen et al., 2007). Protein midpoint melting temperatures (T_m) were assayed using the LightCycler480 System II (Roche), using the following program: 30 s at 20°C, ramp up to 85°C at 0.06°C/seconds, 30 s at 20°C, excitation wavelength 483 nm, and emission wavelength 568 nm. Using SYPRO Orange (Sigma-Aldrich), an environment-sensitive dye that interacts with hydrophobic amino acid residues, the melting of a protein can be observed as a fluorescence increase when the hydrophobic core residues of a protein fold undergo exposure to the dye as the protein unfolds. SYPRO Orange dye interacts with these exposed hydrophobic regions causing an increase in fluorescence. The maximum or minimum of a first derivative curve of the fluorescence profile indicates the T_m.

Crystallization, X-Ray Diffraction Data Collection, and Structure Determination

Crystals of Mt-CCR2 and Ph-CCR1 were grown by vapor diffusion at 4°C in hanging drops, which consisted of 1 μL of protein in storage buffer (500 μM SeMet-labeled Mt-CCR2 plus 1.5 mM NADPH; or 10 mg/mL Ph-CCR1 plus 5 mM $NADP^+$ [Sigma-Aldrich] or 0.2 M sodium iodide) mixed with 1 μL crystallization reservoir (21% [w/v] polyethylene glycol 8000, 0.2 M potassium acetate, 100 mM HEPES [pH 7.5], and 2 mM DTT for Mt-CCR2; or 21% [w/v] polyethylene glycol 3350, 0.3 M calcium acetate, 100 mM sodium succinate [pH 5.5], and 2 mM DTT for Ph-CCR1).

Crystals of Mt-CAD2 and its Lys169Ala mutant were grown using sitting drop vapor diffusion method with 2 μL protein (20 mg/mL) and 2-μL reservoir solutions (25% polyethylene glycol 3350 and 0.1 M Bis-Tris, pH 6.5) at 4°C. Seeding was used to improve the quality and size of the crystals, which grew to 0.3 × 0.2 × 0.1 mm.

Prior to freezing at −168°C, crystals of Mt-CCR2 and Ph-CCR1 were soaked for 3 min in cryoprotectant (crystallization reservoir supplemented with 10 to 17% [v/v] ethylene glycol). X-ray diffraction data were collected on an ADSC Quantum 4 CCD detector at beamline 9-2 of the Stanford Synchrotron Radiation Laboratory) or on ADSC Q315 CCD detectors at beamlines 8.2.1 and 8.2.2 of the Advanced Light Source, Lawrence Berkeley National Laboratory. For Mt-CAD2 and its Lys169Ala mutant, the crystals were flash frozen at −180°C for data collection with a conventional x-ray source (RU-H3R) and R axis IV++ image plate detector.

Diffraction data were indexed, integrated, and scaled with HKL2000 (Otwinowski and Minor, 1997), or MOSFLM (Battye et al., 2011) and SCALA (Evans, 2006). Mt-CCR2 and Ph-CCR1/$NADP^+$ were crystallized in space group $P2_12_12$ and $P2_12_12_1$, respectively, with two monomers in the asymmetric unit. Apo-Ph-CCR1 was crystallized in space group $P6_122$ and with a single monomer in the asymmetric unit. The crystals of Mt-CAD2 belong to space group $P2_12_12_1$ with one Mt-CAD2 molecule in the crystallographic asymmetric unit.

Initial crystallographic phases for Mt-CCR2 were determined from multiwavelength anomalous dispersion. The positions of the two selenium sites per Mt-CCR2 monomer, experimental multiwavelength anomalous dispersion phases, and density modification improved phases were obtained with the program CNS (Brünger et al., 1998). Electron density maps calculated with the initial phases allowed manual building with the program O (Jones et al., 1991) of a 60% complete atomic model of Mt-CCR2, which was subsequently improved through automated building with the program ARP/wARP (Perrakis et al., 1999) and then iterations of manual building and CNS refinement. In the final Mt-CCR2 structure, residues A81-A86, B82-B89, A315-A323, and B318-B323 are disordered.

The structures of Ph-CCR1 were determined through molecular replacement analysis with the Molrep program (Vagin and Teplyakov, 2010). The starting coordinate sets for molecular replacement searches were: for the orthorhombic crystal form, a homology model constructed with the Modeler program (Sali and Blundell, 1993) and a Mt-CCR2 template; and for the hexagonal crystal form, a refined structure of orthorhombic Ph-CCR1. The ARP/wARP program was used for automated rebuilding of the initial models. Subsequent structural refinements utilized the CNS and Phenix (Adams et al., 2010) programs. Xfit (McRee, 1999) and Coot (Emsley and Cowtan, 2004) were used for graphical map inspection and manual rebuilding of atomic models. In all Ph-CCR1 structures, the first three amino acid residues at the N terminus and the last 10 to 11 residues at the C terminus were not observed.

The structure of Mt-CAD2 was solved by molecular replacement using the program PHASER (McCoy et al., 2007) and the DFR structure (PDB ID: 2C29) (Petit et al., 2007) as a search model. Interactive model building

used the program Coot. Crystallographic refinement used the program CNS. Water molecules were added with program ARP/wARP (Lamzin et al., 2001) and verified manually. In the Mt-CAD2 model, the first five amino acid residues in the N terminus were not observed. The structure of Mt-CAD2 mutant Lys169Ala was determined using the refined Mt-CAD2 structure as the starting model, and model building and refinement were performed with the same approach and programs. In the mutant model, the first seven amino acid residues in the N terminus and a region between residues 88 and 93 were disordered.

The programs PROCHECK (Laskowski et al., 1993) and MolProbity (Chen et al., 2010) were used to check the stereochemistry quality of the models. For Mt-CCR2 structure, all residues except Ile-191 in molecule B are within allowed regions of the Ramachandran plot. For structures of both Ph-CCR1 and Mt-CAD2, all backbone ϕ-ψ torsion angles are within allowed regions of the Ramachandran plot. For the generation of omit electron density maps (Figures 3 and 5), the atoms of interest were deleted from the atomic model, and the resultant partial structure was subjected to a single full round of refinement prior to use in the calculation of map coefficients. A summary of crystallographic data collection and refinement statistics for Ph-CCR1, Mt-CCR2, and Mt-CAD2 is presented in Supplemental Table 2.

Molecular Modeling and Docking

For molecular docking of NADPH and substrate to Mt-CAD2, the program GOLD (Jones et al., 1997) was utilized, with the Mt-CAD2 active site defined by the catalytic residue Tyr-165. Default genetic algorithm parameters were used for controlling the operation of the docking process. The lowest energy docking results were identified according to the GOLD-score. The optimal binding mode was identified by analysis of the hydrogen bonds and van der Waals contacts between enzyme and ligands. Minor adjustments of the GOLD solution were manually made using the program COOT, in reference to the DFR structure in complex with $NADP^+$ and with substrates (PDB ID: 2C29).

For homology modeling of Mt-CAD1, the template structure At-CAD5 (PDBID: 2CF5) was used with the comparative modeling program MODELER (Martí-Renom et al., 2000), which generates a model through optimal satisfaction of spatial restraints derived from the structural template and standard energy terms. The cosubstrate NADPH and substrate were also docked into the Mt-CAD1 active site using an approach similar to that described above.

Accession Numbers

Atomic coordinates and structure factors have been deposited to the Research Collaboratory for Structural Bioinformatics Protein Data Bank with the accession codes 4R1S (Ph-CCR1/$NADP^+$), 4R1T (apo-Ph-CCR1), 4R1U (Mt-CCR2), 4QTZ (Mt-CAD2), and 4QUK (Mt-CAD2-Lys169Ala). Sequence data from this article can be found in the GenBank/EMBL database under the following accession numbers: AHX56186.1 (Ph-CCR1), XM_003604190.1 (Mt-CCR2), KEH44099.1 (Mt-CAD1), and ACJ85556.1 (Mt-CAD2).

Supplemental Data

The following materials are available in the online version of this article.

Supplemental Figure 1. Sequence Alignment of Selected SDR Enzymes.

Supplemental Figure 2. Structural Comparison of Wild-Type and Lys169Ala Mutant Forms of Mt-CAD2.

Supplemental Figure 3. Modeled Structure of Mt-CAD1.

Supplemental Figure 4. Molecular Surfaces of $NADP^+$-Bound Ph-CCR1 and Apo Forms of Mt-CCR2 and Mt-CAD2.

Supplemental Table 1. Nucleotide Sequences of Primers Used in the Generation of Expression Vectors for CCR and CAD Proteins.

Supplemental Table 2. Summary of Data Collection and Refinement Statistics.

ACKNOWLEDGMENTS

We thank Lloyd Sumner and He Li for critical reading of the article and support staff at the Berkeley Center for Structural Biology and Advanced Light Source, Stanford Synchrotron Radiation Laboratory, and Structural Biology Center beamline 19ID at the Advanced Photon Source, Argonne National Laboratory (Argonne, IL) for assistance with data collection. Argonne is operated by UChicago Argonne for the U.S. Department of Energy, Office of Biological and Environmental Research under Contract DE-AC02-06CH11357. The Berkeley Center for Structural Biology is supported in part by the National Institutes of Health, National Institute of General Medical Sciences, and the Howard Hughes Medical Institute. The Advanced Light Source is supported by the Director, Office of Science, Office of Basic Energy Sciences, of the U.S. Department of Energy under Contract DE-AC02-05CH11231. This work was supported by Oklahoma Center for the Advancement of Science and Technology Grant PSB11-033 to X.W., U.S. Department of Energy Feedstock Genomics program Grant DE-FG02-06ER64303 to R.A.D., the Samuel Roberts Noble Foundation to X.W. and R.A.D., by National Science Foundation Grant EEC-0813570 to J.P.N., and by National Science Foundation Grant MCB-0919987 to N.D. J.P.N. is an investigator with the Howard Hughes Medical Institute.

AUTHOR CONTRIBUTIONS

J.P.N., X.W., N.D., and R.A.D. designed research. H.P., R.Z., G.V.L., J.K.M., E.K.B., and M.E.B. performed research. H.P., R.Z., G.V.L., and X.W. analyzed data. G.V.L, H.P., J.P.N., and X.W. wrote the article. J.P.N. and X.W. made equal contributions to coordinate this work.

Received May 5, 2014; revised July 27, 2014; accepted August 8, 2014; published September 12, 2014.

REFERENCES

Adams, P.D., et al. (2010). PHENIX: a comprehensive Python-based system for macromolecular structure solution. Acta Crystallogr. D Biol. Crystallogr. **66:** 213–221.

Anterola, A.M., and Lewis, N.G. (2002). Trends in lignin modification: a comprehensive analysis of the effects of genetic manipulations/mutations on lignification and vascular integrity. Phytochemistry **61:** 221–294.

Baltas, M., Lapeyre, C., Bedos-Belval, F., Maturano, M., Saint-Aguet, P., Roussel, L., Duran, H., and Grima-Pettenati, J. (2005). Kinetic and inhibition studies of cinnamoyl-CoA reductase 1 from *Arabidopsis thaliana*. Plant Physiol. Biochem. **43:** 746–753.

Barakat, A., Yassin, N.B., Park, J.S., Choi, A., Herr, J., and Carlson, J.E. (2011). Comparative and phylogenomic analyses of cinnamoyl-CoA reductase and cinnamoyl-CoA-reductase-like gene family in land plants. Plant Sci. **181:** 249–257.

Barakat, A., Bagniewska-Zadworna, A., Choi, A., Plakkat, U., DiLoreto, D.S., Yellanki, P., and Carlson, J.E. (2009). The cinnamyl alcohol dehydrogenase gene family in Populus: phylogeny, organization, and expression. BMC Plant Biol. **9:** 26.

Battye, T.G., Kontogiannis, L., Johnson, O., Powell, H.R., and Leslie, A.G. (2011). iMOSFLM: a new graphical interface for diffraction-image processing with MOSFLM. Acta Crystallogr. D Biol. Crystallogr. **67:** 271–281.

Baucher, M., Halpin, C., Petit-Conil, M., and Boerjan, W. (2003). Lignin: genetic engineering and impact on pulping. Crit. Rev. Biochem. Mol. Biol. **38:** 305–350.

Boatright, J., Negre, F., Chen, X., Kish, C.M., Wood, B., Peel, G., Orlova, I., Gang, D., Rhodes, D., and Dudareva, N. (2004). Understanding in vivo benzenoid metabolism in petunia petal tissue. Plant Physiol. **135:** 1993–2011.

Boerjan, W., Ralph, J., and Baucher, M. (2003). Lignin biosynthesis. Annu. Rev. Plant Biol. **54:** 519–546.

Bomati, E.K., and Noel, J.P. (2005). Structural and kinetic basis for substrate selectivity in *Populus tremuloides* sinapyl alcohol dehydrogenase. Plant Cell **17:** 1598–1611.

Boudet, A.M., Lapierre, C., and Grima-Pettenati, J. (1995). Tansley review No. 80. Biochemistry and molecular biology of lignification. New Phytol. **129:** 203–236.

Breton, R., Housset, D., Mazza, C., and Fontecilla-Camps, J.C. (1996). The structure of a complex of human 17beta-hydroxysteroid dehydrogenase with estradiol and $NADP^+$ identifies two principal targets for the design of inhibitors. Structure **4:** 905–915.

Brünger, A.T., et al. (1998). Crystallography & NMR system: A new software suite for macromolecular structure determination. Acta Crystallogr. D Biol. Crystallogr. **54:** 905–921.

Campbell, M.M., and Sederoff, R.R. (1996). Variation in lignin content and composition. Mechanisms of control and implications for the genetic improvement of plants. Plant Physiol. **110:** 3–13.

Carugo, O., and Argos, P. (1997). NADP-dependent enzymes. I: Conserved stereochemistry of cofactor binding. Proteins **28:** 10–28.

Chen, F., and Dixon, R.A. (2007). Lignin modification improves fermentable sugar yields for biofuel production. Nat. Biotechnol. **25:** 759–761.

Chen, V.B., Arendall, W.B., III., Headd, J.J., Keedy, D.A., Immormino, R.M., Kapral, G.J., Murray, L.W., Richardson, J.S., and Richardson, D.C. (2010). MolProbity: all-atom structure validation for macromolecular crystallography. Acta Crystallogr. D Biol. Crystallogr. **66:** 12–21.

Clermont, S., Corbier, C., Mely, Y., Gerard, D., Wonacott, A., and Branlant, G. (1993). Determinants of coenzyme specificity in glyceraldehyde-3-phosphate dehydrogenase: role of the acidic residue in the fingerprint region of the nucleotide binding fold. Biochemistry **32:** 10178–10184.

Costa, M.A., Collins, R.E., Anterola, A.M., Cochrane, F.C., Davin, L.B., and Lewis, N.G. (2003). An in silico assessment of gene function and organization of the phenylpropanoid pathway metabolic networks in *Arabidopsis thaliana* and limitations thereof. Phytochemistry **64:** 1097–1112.

Damiani, I., Morreel, K., Danoun, S., Goeminne, G., Yahiaoui, N., Marque, C., Kopka, J., Messens, E., Goffner, D., Boerjan, W., Boudet, A.M., and Rochange, S. (2005). Metabolite profiling reveals a role for atypical cinnamyl alcohol dehydrogenase CAD1 in the synthesis of coniferyl alcohol in tobacco xylem. Plant Mol. Biol. **59:** 753–769.

Danehy, J.P., Doherty, B.T., and Egan, C.P. (1971). The oxidation of organic divalent sulfur by iodine. 11. The equilibrating thiol-iodine-disulfide-hydrogen iodide system in acetic acid and evidence for sulfenyl iodide intermediates. J. Org. Chem. **36:** 2525–2530.

Davin, L.B., and Lewis, N.G. (1992). Phenylpropanoid metabolism: biosynthesis of monolignols, lignans and neolignans, lignins and suberins. Recent Adv. Phytochem. **26:** 325–375.

Deacon, A.M., Ni, Y.S., and Coleman, W.G., Jr., andEalick, S.E. (2000). The crystal structure of ADP-L-glycero-D-mannoheptose 6-epimerase: catalysis with a twist. Structure **8:** 453–462.

Dixon, R.A., Chen, F., Guo, D., and Parvathi, K. (2001). The biosynthesis of monolignols: a "metabolic grid", or independent pathways to guaiacyl and syringyl units? Phytochemistry **57:** 1069–1084.

Donaldson, L.A. (2001). Lignification and lignin topochemistry - an ultrastructural view. Phytochemistry **57:** 859–873.

Doublié, S. (1997). Preparation of selenomethionyl proteins for phase determination. Methods Enzymol. **276:** 523–530.

Ebel, J., and Grisebach, H. (1973). Reduction of cinnamic acids to cinnamyl alcohols with an enzyme preparation from cell suspension cultures of soybean (*Glycine max*). FEBS Lett. **30:** 141–143.

Emsley, P., and Cowtan, K. (2004). Coot: model-building tools for molecular graphics. Acta Crystallogr. D Biol. Crystallogr. **60:** 2126–2132.

Escamilla-Treviño, L.L., Shen, H., Uppalapati, S.R., Ray, T., Tang, Y., Hernandez, T., Yin, Y., Xu, Y., and Dixon, R.A. (2010). Switchgrass (*Panicum virgatum*) possesses a divergent family of cinnamoyl CoA reductases with distinct biochemical properties. New Phytol. **185:** 143–155.

Evans, P. (2006). Scaling and assessment of data quality. Acta Crystallogr. D Biol. Crystallogr. **62:** 72–82.

Filling, C., Berndt, K.D., Benach, J., Knapp, S., Prozorovski, T., Nordling, E., Ladenstein, R., Jörnvall, H., and Oppermann, U. (2002). Critical residues for structure and catalysis in short-chain dehydrogenases/reductases. J. Biol. Chem. **277:** 25677–25684.

Gargouri, M., Manigand, C., Maugé, C., Granier, T., Langlois d'Estaintot, B., Cala, O., Pianet, I., Bathany, K., Chaudière, J., and Gallois, B. (2009). Structure and epimerase activity of anthocyanidin reductase from *Vitis vinifera*. Acta Crystallogr. D Biol. Crystallogr. **65:** 989–1000.

Goffner, D., Van Doorsselaere, J., Yahiaoui, N., Samaj, J., Grima-Pettenati, J., and Boudet, A.M. (1998). A novel aromatic alcohol dehydrogenase in higher plants: molecular cloning and expression. Plant Mol. Biol. **36:** 755–765.

Gourley, D.G., Shrive, A.K., Polikarpov, I., Krell, T., Coggins, J.R., Hawkins, A.R., Isaacs, N.W., and Sawyer, L. (1999). The two types of 3-dehydroquinase have distinct structures but catalyze the same overall reaction. Nat. Struct. Biol. **6:** 521–525.

Jez, J.M., Bowman, M.E., Dixon, R.A., and Noel, J.P. (2000). Structure and mechanism of the evolutionarily unique plant enzyme chalcone isomerase. Nat. Struct. Biol. **7:** 786–791.

Jones, G., Willett, P., Glen, R.C., Leach, A.R., and Taylor, R. (1997). Development and validation of a genetic algorithm for flexible docking. J. Mol. Biol. **267:** 727–748.

Jones, T.A., Zou, J.-Y., Cowan, S.W., and Kjeldgaard, M. (1991). Improved methods for building protein models in electron density maps and the location of errors in these models. Acta Crystallogr. A **47:** 110–119.

Jörnvall, H., Persson, M., and Jeffery, J. (1981). Alcohol and polyol dehydrogenases are both divided into two protein types, and structural properties cross-relate the different enzyme activities within each type. Proc. Natl. Acad. Sci. USA **78:** 4226–4230.

Jörnvall, H., Hedlund, J., Bergman, T., Oppermann, U., and Persson, B. (2010). Superfamilies SDR and MDR: from early ancestry to present forms. Emergence of three lines, a Zn-metalloenzyme, and distinct variabilities. Biochem. Biophys. Res. Commun. **396:** 125–130.

Jörnvall, H., Persson, B., Krook, M., Atrian, S., Gonzàlez-Duarte, R., Jeffery, J., and Ghosh, D. (1995). Short-chain dehydrogenases/reductases (SDR). Biochemistry **34:** 6003–6013.

Kamitori, S., Iguchi, A., Ohtaki, A., Yamada, M., and Kita, K. (2005). X-ray structures of NADPH-dependent carbonyl reductase from Sporobolomyces salmonicolor provide insights into stereoselective reductions of carbonyl compounds. J. Mol. Biol. **352:** 551–558.

Kim, S.J., Kim, M.R., Bedgar, D.L., Moinuddin, S.G., Cardenas, C.L., Davin, L.B., Kang, C., and Lewis, N.G. (2004). Functional reclassification of the putative cinnamyl alcohol dehydrogenase multigene family in Arabidopsis. Proc. Natl. Acad. Sci. USA **101:** 1455–1460.

Klempien, A., et al. (2012). Contribution of CoA ligases to benzenoid biosynthesis in petunia flowers. Plant Cell **24:** 2015–2030.

Kraulis, P.J. (1991). MOLSCRIPT: a program to produce both detailed and schematic plots of protein structures. J. Appl. Crystallogr. **24:** 946–950.

Lamzin, V.S., Perrakis, A., and Wilson, K.S. (2001). The ARP/WARP suite for automated construction and refinement of protein models. In Int. Tables for Crystallography: Crystallography of Biological Macromolecules, M.G. Rossmann and E. Arnold, eds (Dordrecht/Boston/London: Kluwer Academic Publishers), pp. 720–722.

Laskowski, R.A., MacArthur, M.W., Moss, D.S., and Thornton, J.M. (1993). PROCHECK - a program to check the stereochemical quality of protein structures. J. Appl. Crystallogr. **26:** 283–291.

Lauvergeat, V., Lacomme, C., Lacombe, E., Lasserre, E., Roby, D., and Grima-Pettenati, J. (2001). Two cinnamoyl-CoA reductase (CCR) genes from *Arabidopsis thaliana* are differentially expressed during development and in response to infection with pathogenic bacteria. Phytochemistry **57:** 1187–1195.

Lee, Y., Chen, F., Gallego-Giraldo, L., Dixon, R.A., and Voit, E.O. (2011). Integrative analysis of transgenic alfalfa (*Medicago sativa* L.) suggests new metabolic control mechanisms for monolignol biosynthesis. PLOS Comput. Biol. **7:** e1002047.

Lewis, N.G., and Yamamoto, E. (1990). Lignin: occurrence, biogenesis and biodegradation. Annu. Rev. Plant Physiol. Plant Mol. Biol. **41:** 455–496.

Li, L., Cheng, X., Lu, S., Nakatsubo, T., Umezawa, T., and Chiang, V.L. (2005). Clarification of cinnamoyl co-enzyme A reductase catalysis in monolignol biosynthesis of aspen. Plant Cell Physiol. **46:** 1073–1082.

Lüderitz, T., and Grisebach, H. (1981). Enzymic synthesis of lignin precursors. Comparison of cinnamoyl-CoA reductase and cinnamyl alcohol:NADP$^+$ dehydrogenase from spruce (*Picea abies* L.) and soybean (*Glycine max* L.). Eur. J. Biochem. **119:** 115–124.

Mansell, R.L., Gross, G.G., Stöckigt, J., Franke, H., and Zenk, M.H. (1974). Purification and properties of cinnamyl alcohol dehydrogenase from higher plants involved in lignin biosynthesis. Phytochemistry **13:** 2427–2435.

Martí-Renom, M.A., Stuart, A.C., Fiser, A., Sánchez, R., Melo, F., and Sali, A. (2000). Comparative protein structure modeling of genes and genomes. Annu. Rev. Biophys. Biomol. Struct. **29:** 291–325.

McCoy, A.J., Grosse-Kunstleve, R.W., Adams, P.D., Winn, M.D., Storoni, L.C., and Read, R.J. (2007). Phaser crystallographic software. J. Appl. Cryst. **40:** 658–674.

McKinley-McKee, J.S., Winberg, J.O., and Pettersson, G. (1991). Mechanism of action of *Drosophila melanogaster* alcohol dehydrogenase. Biochem. Int. **25:** 879–885.

McRee, D.E. (1999). XtalView/Xfit—A versatile program for manipulating atomic coordinates and electron density. J. Struct. Biol. **125:** 156–165.

Mellerowicz, E.J., Baucher, M., Sundberg, B., and Boerjan, W. (2001). Unravelling cell wall formation in the woody dicot stem. Plant Mol. Biol. **47:** 239–274.

Moummou, H., Kallberg, Y., Tonfack, L.B., Persson, B., and van der Rest, B. (2012). The plant short-chain dehydrogenase (SDR) superfamily: genome-wide inventory and diversification patterns. BMC Plant Biol. **12:** 219.

Niesen, F.H., Berglund, H., and Vedadi, M. (2007). The use of differential scanning fluorimetry to detect ligand interactions that promote protein stability. Nat. Protoc. **2:** 2212–2221.

Otwinowski, Z., and Minor, W. (1997). Processing of x-ray diffraction data collected in oscillation mode. In Methods in Enzymology, C.W. Carter and R.M. Sweet, eds (New York: Academic Press), pp. 307–326.

Perrakis, A., Morris, R., and Lamzin, V.S. (1999). Automated protein model building combined with iterative structure refinement. Nat. Struct. Biol. **6:** 458–463.

Petit, P., Granier, T., d'Estaintot, B.L., Manigand, C., Bathany, K., Schmitter, J.M., Lauvergeat, V., Hamdi, S., and Gallois, B. (2007). Crystal structure of grape dihydroflavonol 4-reductase, a key enzyme in flavonoid biosynthesis. J. Mol. Biol. **368:** 1345–1357.

Ravilious, G.E., Nguyen, A., Francois, J.A., and Jez, J.M. (2012). Structural basis and evolution of redox regulation in plant adenosine-5′-phosphosulfate kinase. Proc. Natl. Acad. Sci. USA **109:** 309–314.

Rossmann, M.G., Liljas, A., Branden, C.-I., and Bansazak, L.J. (1975). Evolutionary and Structural Relationships among Dehydrogenases. (New York: Academic Press).

Ryu, S.E. (2012). Structural mechanism of disulphide bond-mediated redox switches. J. Biochem. **151:** 579–588.

Sali, A., and Blundell, T.L. (1993). Comparative protein modelling by satisfaction of spatial restraints. J. Mol. Biol. **234:** 779–815.

Shao, H., Dixon, R.A., and Wang, X. (2007). Crystal structure of vestitone reductase from alfalfa (*Medicago sativa* L.). J. Mol. Biol. **369:** 265–276.

Sibout, R., Eudes, A., Mouille, G., Pollet, B., Lapierre, C., Jouanin, L., and Séguin, A. (2005). CINNAMYL ALCOHOL DEHYDROGENASE-C and -D are the primary genes involved in lignin biosynthesis in the floral stem of Arabidopsis. Plant Cell **17:** 2059–2076.

Sonawane, P., Vishwakarma, R.K., and Khan, B.M. (2013). Biochemical characterization of recombinant cinnamoyl CoA reductase 1 (LI-CCRH1) from *Leucaena leucocephala*. Int. J. Biol. Macromol. **58:** 154–159.

Tanaka, N., Nonaka, T., Nakamura, K.T., and Hara, A. (2001). SDR: structure, mechanism of action, and substrate recognition. Curr. Org. Chem. **5:** 89–111.

Tu, Y., Rochfort, S., Liu, Z., Ran, Y., Griffith, M., Badenhorst, P., Louie, G.V., Bowman, M.E., Smith, K.F., Noel, J.P., Mouradov, A., and Spangenberg, G. (2010). Functional analyses of caffeic acid O-methyltransferase and Cinnamoyl-CoA-reductase genes from perennial ryegrass (*Lolium perenne*). Plant Cell **22:** 3357–3373.

Vagin, A., and Teplyakov, A. (2010). Molecular replacement with MOLREP. Acta Crystallogr. D Biol. Crystallogr. **66:** 22–25.

Valencia, E., Larroy, C., Ochoa, W.F., Parés, X., Fita, I., and Biosca, J.A. (2004). Apo and Holo structures of an NADPH-dependent cinnamyl alcohol dehydrogenase from *Saccharomyces cerevisiae*. J. Mol. Biol. **341:** 1049–1062.

Vanholme, R., et al. (2013). Caffeoyl shikimate esterase (CSE) is an enzyme in the lignin biosynthetic pathway in Arabidopsis. Science **341:** 1103–1106.

Wagner, A., Tobimatsu, Y., Goeminne, G., Phillips, L., Flint, H., Steward, D., Torr, K., Donaldson, L., Boerjan, W., and Ralph, J. (2013). Suppression of CCR impacts metabolite profile and cell wall composition in *Pinus radiata* tracheary elements. Plant Mol. Biol. **81:** 105–117.

Wengenmayer, H., Ebel, J., and Grisebach, H. (1976). Enzymic synthesis of lignin precursors. Purification and properties of a cinnamoyl-CoA:

NADPH reductase from cell suspension cultures of soybean (*Glycine max*). Eur. J. Biochem. **65:** 529–536.

Whetten, R., and Sederoff, R. (1995). Lignin biosynthesis. Plant Cell **7:** 1001–1013.

Youn, B., Camacho, R., Moinuddin, S.G., Lee, C., Davin, L.B., Lewis, N.G., and Kang, C. (2006). Crystal structures and catalytic mechanism of the Arabidopsis cinnamyl alcohol dehydrogenases AtCAD5 and AtCAD4. Org. Biomol. Chem. **4:** 1687–1697.

Zhao, Q., et al. (2013). Loss of function of cinnamyl alcohol dehydrogenase 1 leads to unconventional lignin and temperature-sensitive growth reduction in *Medicago truncatula*. Proc. Natl. Acad. Sci. USA **110:** 13660–13665.

Zhou, R., Jackson, L., Shadle, G., Nakashima, J., Temple, S., Chen, F., and Dixon, R.A. (2010). Distinct cinnamoyl CoA reductases involved in parallel routes to lignin in *Medicago truncatula*. Proc. Natl. Acad. Sci. USA **107:** 17803–17808.